Design of a Hydrogel for 3-D Bioprinting Neural Tissue

Michaela Thomas[1*]

Collaborators:
Aspect Biosystems
Sarah Wong[2]
Cory Blood[3]
Stephanie M. Willerth[1,4,5,6]

[1] Department of Mechanical Engineering, University of Victoria, Victoria BC, Canada
[2] Department of Biomedical Engineering, University of Victoria, Victoria BC, Canada
[3] Department of Biochemistry and Microbiology, University of Victoria, Victoria BC, Canada
[4] Division of Medical Sciences, University of Victoria, Victoria BC, Canada
[5] Centre for Biomedical Research, University of Victoria, Victoria, BC, Canada
[6] International Collaboration on Repair Discoveries (ICORD), Vancouver, BC, Canada
***Correspondence: Michaela Thomas** (michaelathomas@uvic.ca)

Assignment presented in partial fulfilment of the requirements for the degree of Master of Engineering (Mechanical) in the Faculty of Engineering at the University of Victoria

Abstract

Neurodegenerative diseases and disorders affect millions of individuals in North America. The annual cost of treatment is in the billions and treatment options remain limited. Current methods focus on physical rehabilitation and drugs to mask declining neuron function. Drug therapies currently available can hide the effects of neuron death but quickly lose their efficacy. Cell therapy for neurodegenerative diseases remains limited because of the difficulty of successfully implanting new tissue into the central nervous system. Development of new drug treatments is similarly stunted because of the imperfection of animal trials and the challenges in growing biomimetic tissue for drug screening. The production of biomimetic neural tissue would allow for large-scale drug discovery and screening. Three-dimensional (3-D) printing offers a streamlined system to engineer cellularly and mechanically accurate neural tissue for drug discovery, or, in the future, for cell therapy. New microfluidic printing platforms such as those designed by Aspect Biosystems offer an increased cellular resolution and printheads which have little impact on cell viability and can print a variety of extrudable polymers such as fibrin, collagen, hyaluronic acid, poly (caprolactone) and poly (ethylene glycol). This work presents the development of an extrudable polymer compatible with Aspect Biosystems 3-D printing technology which supports human-induced pluripotent stem cell differentiation into a neural tissue for use in drug discovery and disease modelling. The polymer bioink is made up of base polymers A and B[*], whose concentrations were optimized to increase cell viability. Additives G, P and L were then added to the formulation and their effects on cell differentiation were quantified. These preliminary studies indicate that polymer B may decrease cell proliferation while additive L may increase the number of cells destined for a neuronal fate. Future studies should focus on long-term cell differentiation and replicates.

* All reagents and concentrations in the bioink are the intellectual property of Aspect Biosystems and will not be revealed in the course of this report.

Contents

1.0 Introduction 1
2.0 Literature review 2
2.1 In vitro neural cell culture 2
2.2 History of bioinks 3
2.3 Bioprinting neural tissue 4
3.0 Materials and methods 7
3.1 Expansion and maintenance of NPCs 7
3.2 Preparation of bioink samples for mechanical analysis ..... **Error! Bookmark not defined.**
3.3 Scanning electron microscopy 8
3.4 Rheology ..... **Error! Bookmark not defined.**
3.5 Sample formulations for biological analysis 8
3.6 Flow cytometry 9
3.6.1 Preparation of cell suspension 9
3.6.2 ViaCount assay 9
3.6.2 Staining 9
3.6.3 Flow cytometry analysis 10
3.7 Immunocytochemistry 10
4.0 Results and Discussion 11
4.1 Optimizing additive G concentration 11
4.2 Characterizing mechanical properties 13
4.2.1 Scanning electron microscope imaging 13
4.2.2 Rheological analysis ..... **Error! Bookmark not defined.**
4.3 Biological analysis 15
5.0 Conclusion and future work 21
6.0 Conflict of interest 21
7.0 Funding 21
8.0 References 22
9.0 Appendix 1 28

List of Figures

Figure 4: Cells stained with DAPI, TUJ1, and SOX2 24 days after printing. 5
Figure 5: Cortical neurons 5 days post printing seeded in a peptide modified gellan gum 6
Figure 6: Polymerization speeds of bioinks with varying concentrations of additive G. 12
Figure 7: Average time of bioink degradation in days with increasing concentrations of additive G. 12
Figure 8: SEM images of bioink samples formulated with hydrogel A. 13
Figure 9: SEM images of bioink samples with hydrogel A. 14
Figure 10: SEM images of bioink samples with hydrogel A and B. 14
Figure 11: Storage and loss moduli of bioink samples formulated with hydrogel A. **Error! Bookmark not defined.**
Figure 12: Storage and loss moduli of bioink samples formulated with hydrogel A. **Error! Bookmark not defined.**
Figure 13: Storage (solid markers) and loss (bordered markers) moduli of bioink samples prepared with Hydrogel A. ..... **Error! Bookmark not defined.**
Figure 14: Storage (solid markers) and loss (bordered markers) moduli of bioink samples prepared with Hydrogel A. ..... **Error! Bookmark not defined.**
Figure 15: Cell viability 24 hours after printing in each formulation. Viability ranged from 35-99%. 15
Figure 16: Cell viability 24 hours after printing according to bioink constituents. 16
Figure 15: Samples of bioink formulation 1 (hydrogel A with concentration 1 of additive G) 17
Figure 16: Samples of bioink formulation 5 (hydrogel A with concentration 1 of additive G and additive L) 17
Figure 17: Percentage of cells positive for TUJ1 18
Figure 18: Percentage of cells positive for TUJ1 19
Figure 19: Cells 14 days after printing in hydrogel A 20
Figure 20: Cells 14 days after printing. 20

List of Tables

Table 1: Bioink formulations 9
Table 2: Antibodies and isotypes used for flow cytometry. 10
Table 3: Primary antibodies and conjugates for ICC. 11
Table A 1: Bioprinting neural tissue by a variety of printing methods using different cell types. 28
Table A 2: Plate 1 for flow cytometry. 28
Table A 3: Plate 2 for flow cytometry. 28
Table A 4: Flow cytometry on bioink samples 7 days after printing to quantify the cells positive for TUJ1, Nestin and Olig2 29
Table A 5: Comparison of cells positive for Tuj1, Nestin, and Olig-2 in each bioink formulation. 30

List of acronyms

CNS – central nervous system
hESCs – human embryonic stem cells
MSCs – mesenchymal stem cells
NSPCs – neural stem/progenitor cells
hiPSCs – human induced pluripotent stem cells
CRISPER – clustered regularly interspaced short palindromic repeats
PEG – polyethylene glycol
PLGA – poly(lactic-co-glycolic acid)
EBs – embryonic bodies
ECM – extracellular matrix
CAD – computer-aided design
FDS – fused deposition modelling
SLS – selective laser sintering
PCL – polycaprolactone
PLLA – poly(L-lactic acid)
PLO – poly-L-orinthe
PBS – phosphate buffered saline
SEM – scanning electron microscopy
HDMS – hexamethyldisilazane
BSC – biosafety cabinet
FBS – fetal bovine serum

1.0 Introduction

In North America, more than 55 million individuals are treated for neurodegenerative diseases annually. This represents a multi-billion-dollar burden to the healthcare industry for costs associated with treatment and rehabilitation therapy [1]. Selective cell loss in the central nervous system (CNS) often leads to or is a hallmark of the progression of neurodegenerative diseases.

Diseases such as Alzheimer's, Parkinson's, Huntington's, Multiple Sclerosis, and Amyotrophic Lateral Sclerosis; and disorders such as traumatic brain injury, all result in cell loss in targeted areas of the brain [2], making them potential candidates for cell therapy. Cell therapy has the potential to treat neurodegenerative disease by replacing damaged tissues or augmenting remaining cell function [3]. The foundation of cell therapy is that living human cell can be implanted into a damaged region of the body to instigate healing [4]. Neuronal cells possess low regenerative capacity as they do not proliferate after maturation, meaning that the CNS has little capability to self-heal [5]. Cell therapy can work directly to replace damaged neuronal and support cells, or indirectly by secreting soluble factors to facilitate the repair process [6].

Current treatments for neurodegenerative diseases focus primarily on assuaging physical, mental and emotional systems, while cell therapy has the potential to promote cellular repair and remodeling, resulting in improved performance. Several setbacks must be overcome before cell therapy can become the standard. These include methods of ensuring that the proper quantity and type of cells are being generated, particularly when using stem cells as they are pluripotent and developing high-throughput methods for growing neural culture [7] [8]. Direct cell transplantation into the damaged CNS has been done but often these cells fail to functionally integrate into the brain [8].

Bioprinting, the use of 3-D printing techniques with biocompatible materials, cells, or growth factors to create biocompatible devices or living tissue constructs, can be used to manufacture human neural tissue in a consistent, rapid, manner. By 3-D bioprinting living cells a tissue construct can be developed with a close degree of spatial control in terms of biological and mechanical properties. This technology allows for a one-step development of neural tissue constructs in complex geometries.

Engineered biomaterial microenvironments can overcome low cell survival rates once implanted into the damaged CNS and limit migration of cells from the implantation site as well as providing a controlled setting for cell growth and differentiation [7] [9]. The biomaterial scaffolds utilised in 3-D printing are often termed bioinks [10]. These bioinks degrade as the seeded cells develop, either through hydrolysis, or through enzymatic degradation by by-product proteases, leaving a biologically accurate tissue construct [11].

Cells that have been evaluated *in vitro* and *in vivo* for neural regeneration include human embryonic stem cells (hESCs), which are pluripotent stem cells derived from a human embryo; mesenchymal stem cells (MSCs), Schwann cells, which are multipotent stromal cells that can differentiate into osteoblasts, chondrocytes, myocytes, and adipocytes; Schwann cells, which are the primary nervous cell in the peripheral nervous system; neural stem/progenitor stem cells (NSPCs), which are multipotent and can differentiate into neurons, astrocytes and oligodendrocytes; and human induced pluripotent stem cells (hiPSCs), which are adult cells taken back to a pluripotent state [12]. Both hESCs and hiPSCs are pluripotent [13], however hESCs pose a risk of immune rejection after implantation and remain ethically controversial because the blastocyst which they are isolated from does not survive [14]. hiPSCs are adult cells which have been reprogrammed into a pluripotent state using transcription factors [15]. hiPSCs provide a minimum-risk opportunity for cell therapy as they can be derived directly from a patient's own

cells [16]. hiPSCs may also improve drug screening because a patient's cells can be reprogrammed into neural cells which then display disease hallmarks and can create a relevant tissue model [17].

Bioprinting requires a high cell seeding density, therefore the chosen cell line must be capable of constant expansion [18]. Many primary cell types cannot self-renew and are tough to isolate, making pluripotent stem cells an attractive option for bioprinting [18]. Recent genetic advancements such as clustered regularly interspaced short palindromic repeats (CRISPER /Cas9) have made it possible to correct cell mutations in cell lines, making expansion less risky and enhancing the potential for hiPSCs in cell therapy [19]. Cell culture within a scaffold material enhances potential as growing cells can be loaded with chemical factors to control differentiation. 3-D bioprinting of these scaffolds allows close control of the concentration of these chemical factors to encourage cell differentiation in different areas of the construct. Many biomaterials such as polyethylene glycol (PEG) [20], hyaluronan [21], fibrin [21], and alginate [22] have been shown to support neural cell culture in mouse and rat trials. In addition extracellular matrix molecules such as collagen, fibrin, fibronectin and laminin [23] [24] [25] [26] [27] [28]; and polymers such as poly(lactic-co-glycolic acid) (PLGA), N-(2-Hydroxypropyl)methacrylamide (HPMA), and poly (a-hydroxy-acids) [29]; have been used to provide mechanical integrity to the scaffold.

As well as cell therapy, 3-D bioprinted neural tissues can model neurodegenerative diseases and be used for drug discovery. Several groups have produced functional neural tissues [30], but it has required long and labour-intensive culture protocols. Usually the performance of the ensuing tissues is not fully developed, lacking the function of a mature neural network [30]. 3-D bioprinting would allow for the high-throughput production of biologically accurate tissue constructs. This would allow for the creation of large sample sizes and multiple replicates to accurately evaluate cell function and electrophysiology over time both with and without the addition of the drug being researched.

To achieve biomimetic brain tissue constructs for drug screening or disease modelling current bioprinting technologies must be utilized to their full extent to incorporate nutrient flow throughout the cell construct. Functional integration of replacement brain tissue remains a distant goal but begins with accurately producing neural tissue which mimics the mechanical and biochemical conditions found *in vivo*. To do so without inducing inflammation or unplanned cellular responses requires a complex platform with precise controls with regards to sterilization and culture conditions as well as cell and scaffold arrangement.

This work focusses on developing a bioprintable cell scaffold made primarily of polymers A and B which is compatible with microfluidic bioprinting and can support hiPSC differentiation into mature neurons. It aims to optimize additives G, P, and L to support cell viability and printing compatibility.

2.0 Literature review

2.1 *In vitro* neural cell culture

Neural culture platforms exist in two dimensional (2-D) and 3-D. 2-D platforms are effective in inducing neural differentiation from hiPSCs, however the impose unnatural geometric constraints on cells by only allowing free growth in the horizontal direction and not in the vertical direction [31]. The culture protocol to derive neuroepithelial cells from hiPSCs is lengthy and involved. Most commonly it involves the formation of embryonic bodies (EBs) followed by manual isolation of neural rosettes or adherent differentiation in combination with small molecule inhibitors that promote differentiation [32]. This process takes 17-19 days and requires the cells to be passaged several times [32]. Similar conversion rates can be obtained in approximately 6 days by culturing hiPSCs on laminin coated plates in the presence of E6 media [33].

Many researchers have transitioned into culturing cell lines in 3-D systems since 2-D cultures do not exhibit biologically accurate morphology. 3-D cell culture requires suspending cells within a permeable scaffold matrix, resulting in a more physiologically relevant cell microenvironment [31]. It has been found that hiPSC-derived NPCs cultured in 3-D produce more neuronal cells and less astrocytes compared to cells cultured in 2-D [34]. The formation of EBs in a 3-D scaffold allows for cell-cell and cell-scaffold interactions not available in 2-D culture, enabling patterned and structured cell differentiation and morphogenesis [31]. However, in 2-D culture differentiation protocols defined culture conditions are used to ensure lineage [35]. The introduction of a scaffold means that cells will encounter a new set of proteins and biomolecules during growth, which makes it difficult to predict cell behaviour and isolate scaffold effects on differentiation.

2.2 History of bioinks

Neural differentiation of hiPSCs has been evaluated in 3-D scaffolds constructed of a number of biomaterials including fibrin [36], laminin [34], alginate [37], and PEG [38]. Many natural polymers, such as fibrin, laminin, gelatin, and collagen, can be crosslinked under mild conditions into a cytocompatible hydrogel scaffold suitable for 3-D bioprinting [39].

Fibrin scaffolds promote neural adhesion, proliferation, and differentiation, likely because low-concentration fibrin gels possess biochemical and mechanical cues similar to those of brain tissue [40] [41] [42] [43] [44] [45] [36]. Fibrinogen polymerizes under mild conditions with the addition of thrombin but the slow reaction makes it unsuitable for extrusion bioprinting. To reduce polymerization time it is mixed with polysaccharides like alginate to produce a printable bioink [37]. Alginate is one of the most widely employed bioinks and polymerizes quickly with the addition of a divalent cation [10]. Other polysaccharides, such as gellan gum, have similar rates of polymerization [46]. However, these polysaccharides are mostly inert, resulting in limited cell adhesion [10]. Addition of components such as laminin stimulates axonal growth in scaffolds, likely because laminin plays a role in axonal guidance and cell migration in the developing CNS [34]. When fibrin is functionalized with laminin a higher neurite outgrowth is observed than in unmodified fibrin scaffolds [47].

While natural hydrogels retain the biological activity of native extracellular matrix (ECM) molecules, they suffer from batch-to-batch variability and limited possibilities for biochemical modification [48]. In addition, natural hydrogels pose a risk of immunogenicity and disease transfer for clinical applications [48]. In contrast, synthetic hydrogels can be more amenable for biochemical functionalization, such as growth factors, ECM adhesive motifs, and specific molecules agonistic or antagonistic to cell surface receptors; biophysical modulations, including mechanical stiffness, pore size and 3-D architecture; and mimicking key degradation characteristics. Synthetic hydrogels also have a lower risk for immunogenic reactions as their monomers are produced using chemically defined reactions [31]. However, many synthetic scaffold materials require complex reactions for functionalization, which hinders their ability to be bioprinted [49].

The degradation kinetics of the bioink must be well understood because any degradation products may have time to impact the developing or existing tissues [50]. Neural tissue scaffolds generally degrade via hydrolysis, ion exchange, or through enzymatic reactions, over a period of 2-8 weeks. Common byproducts include salts like calcium, protein fragments, or weak acids such as lactic acid [51]. All mid and end-point degradation products must be thoroughly investigated for possible immunogenic reactions. Possible host reactions to the biomaterial include injury, blood-material interactions, inflammation, and development of a fibrous capsule to isolate the foreign material [52].

In comparison to other tissue engineering techniques bioprinting enables the highest control over the arrangement of cells and bioactive nanomaterials in defined scaffold geometries [39]. 3-D printing cell scaffolds means that more effective arrangements can be produced with less effort, achieving constructs with ECM feature size and composition, chemical gradients, varied mechanical properties and specific morphologies that were not previously accessible [53]. 3-D printing has been widely researched for industrial rapid prototyping and additive manufacturing [54]. To begin a print cycle a computer-aided design (CAD) model of the scaffold must be created and features such as cell type and placement and elastic moduli be specified. The program will parse the solid into a stack of cross-sections and print each cross-section layer-by-layer up from the bottom [39].

Microfluidic extrusion continuously extrudes a cell-seeded bioink precursor in tandem with a crosslinking agent [55]. The hydrogel precursors meet in a mixing chamber where polymerization is initiated before deposition, allowing for both easy flow through the nozzle (while the polymer has not set) and a defined structure after printing, when the mixture has polymerized into a semisolid hydrogel [39]. Multiple valves and chambers allow control of flow rate, cell type, and mechanical properties. The computer-guided deposition process is hands-off, allowing for aseptic conditions during printing.

During the printing process cells, experience shear stress and local rheologic forces which influence cell response [39]. Neural cells from any source tend to be delicate and easily disrupted, presenting a major challenge when bioprinting [56]. Physiochemical properties of the scaffold and cytocompatibility for a chosen cell line serve as the two most important factors when designing a bioink [35].

2.3 Bioprinting neural tissue

Neural tissue has been extrusion bioprinted by several groups with varying levels of success (**Table A1**).

Similar to the proposed system by Aspect Biosystems, Gu *et al.* in 2016 extruded a bioink made up of alginate, carboxymethyl-chitosan (CMC) and agarose seeded with frontal cortical human NSCs [57]. Cell viability dropped to 75% immediately after printing, and cell proliferation was highest 11 days post-printing. 21 days post-printing samples stained positive for DAPI and TUJ1, but exhibited little SOX2 expression, indicating that mature neurons (**Figure 4**).

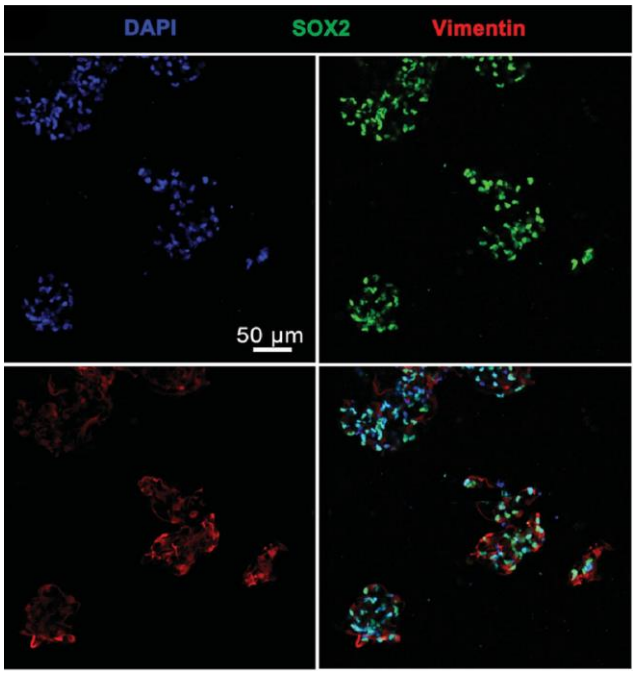

Figure 1: Cells stained with DAPI, TUJ1, and SOX2 24 days after printing. Cells largely expressed both DAPI and TUJ1, indicating mature neurons. Reprinted from (Gu, et al, 2016).

Lozano *et al.* in 2015 extruded a peptide modified gellan gum seeded with primary cortical neurons [46]. 5 days post-printed cells stained positive for TUJ1 and exhibited neuronal cell morphology.

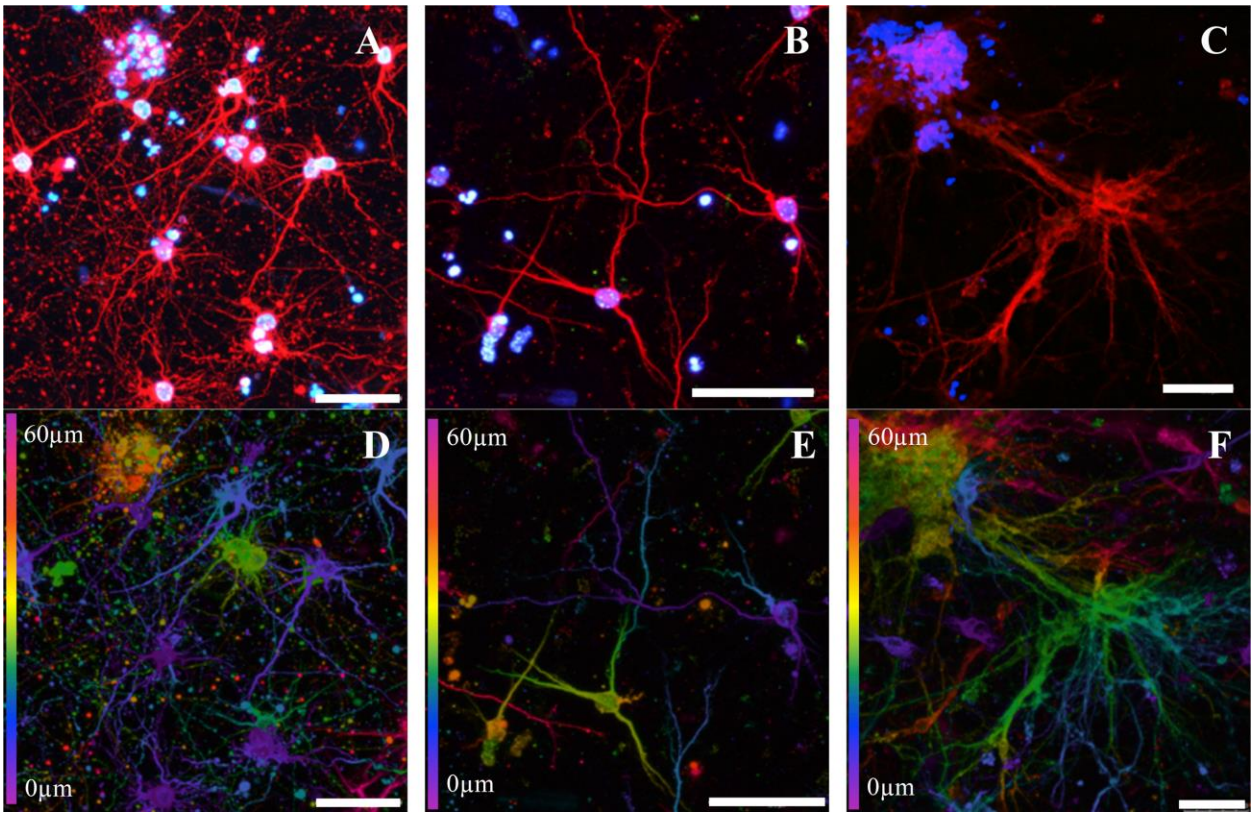

Figure 2: Cortical neurons 5 days post printing seeded in a peptide modified gellan gum at gel concentrations of 0.075%, 0.15% and 0.5% w/v respectively. (a-c) cells stained with β-III (red) for cortical neurons and DAPI (blue) for nuclei. (d-f) depth decoding confocal microscope images of cultures. Colour decoding for the depth of the cells within the gel along the z-axis is given (0-60µm). Different colours represent the different planes along the z-axis. Scale bars represent 50 µm. Reprinted from (Lozano, et al, 2015).

Lee *et al.* in 2010 used extrusion to print collagen and fibrin as well as fibrin loaded with VEGF seeded with murine neural stem cells [58]. Constructs were printed layer-by-layer into a cylindrical shape on a tissue culture dish. Printed cells showed no difference in viability compared to manually plating cells. Cells located up to 1 mm from the fibrin border migrated towards the VEGF-containing fibrin gel, indicating that cells will migrate towards a more permissive region.

These studies differ greatly in the number of cells lost due to the stress of the printing process. Knowing this loss allows the user to seed at the correct cell density. Optimizing the bioink makeup is key to reducing the immediate loss of cell viability post-printing.

Current work indicates that a wide variety of bioink materials may be suitable for 3-D printing neural tissue. However, more research needs to be done comparing the printability of each of these materials in terms of efficiency and ease-of-use, both which become important when scaling up production. This work aimed to develop a bioink consistent with the microfluidic extrusion method used by Aspect Biosystems. It focussed on finding a cohesive unit of bioink and printing method resulting in a high cell viability post-printing and mechanical properties similar to that of natural neural tissue. It could be developed to incorporate a hands-off manner of controlling printing using CAD and microtechnology. This would remove human error and increase the sterility of the system, making it more likely to be used for scale-up for drug testing and disease modelling.

The developed bioink contained two polymer hydrogels, hydrogel A and B, a crosslinking agent, and three additives, G, P, and L. All reagents and concentrations will remain confidential. Hydrogel A was chosen for its ability to support neural cell culture and direct neural differentiation. Hydrogel B was chosen for its rapid polymerization and proven printability. Additives G and P were used to slow the degradation of the bioink in the presence of cells to maintain structural support throughout cell growth. Additive L was chosen because it has been shown to increase neural adhesion and neurite outgrowth. Hydrogel A and B were evaluated for their porosity and mechanical properties while additive G was optimized to minimize polymerization time and maximize time to degradation. Additive P had already been optimized in a previous (unpublished) study. Each additive was evaluated to observe its effect on cell proliferation and differentiation.

3.0 Materials and methods

3.1 Expansion and maintenance of NPCs

hiPSCs were derived from foreskin fibroblasts (iPS(Foreskin)-1, Lot 1-DL-01,WiCell). Media for hiPSCs contains Dulbecco's Modified Eagle Medium (DMEM) High Glucose No Glutamine (Life Technologies), 15% ES-cell qualified fetal bovine serum (FBS) (Life Technologies), 0.1 mM MEM Non-Essential Amino Acids (Life Technologies), 2 mM GlutaMAX™ Supplement (Life Technologies), 0.055 Mm β-mercaptoethanol, 0.1 Mm nucleosides (Millipore Sigma), and 100 µg/mL Penicillin-Streptomycin (Life Technologies).

hiPSCs were differentiated into NPCs using AggreWell 800 plates (Stem Cell) [59]. Plates were prepared by pre-treating wells with AggreWell rinsing solution. 500 µL of rinsing solution was added to each well and the plate was centrifuged at 2000 g for 5 minutes. Rinsing solution was aspirated from the wells. Neural induction medium was prepared, and 1 mL was added to each well. The plate was then centrifuged at 2000 g for 5 minutes and examined under a microscope to ensure that no bubbles remained. If bubbles were still present, the plate was centrifuged a second time.

hiPSC culture was dissociated from wells in a 6-well plate using 3 mL of gentle cell dissociation reagent per well. Dishes were incubated for 10 minutes at 37°C and then cells were dislodged by pipetting up and down. Wells were washed with DMEM and the cell pellet was collected by centrifuging at 300 g for 5 minutes. Cells were resuspended to a final concentration of $3x10^6$ cells/mL and 1 mL of the suspension was added to each well in the AggreWell plate. The plate was then centrifuged at 100 g for 3 minutes to disperse the cells into the microwells. Plates were then incubated at 37°C.

On days 1-5 a partial medium change was performed, removing approximately ¾ of the media and replacing with fresh neural induction medium. On day 6 EBs were replated from the AggreWell plates onto a single well in a 6-well plate. Wells were coated with poly-L-orinthine (PLO) and laminin to increase cellular adhesion. PLO was diluted in phosphate-buffered saline (PBS; Thermo Fisher Scientific) to a final concentration of 15 µg/mL. 1 mL of the solution was added to each well and allowed to incubate for 4 hours at room temperature. The PLO was then aspirated, and the plates were washed twice with PBS and once with DMEM/F-12. Laminin was prepared in DMEM/F-12 to a final concentration of 10 µg/mL and 1 mL was added to each well and allowed to incubate for 4 hours at room temperature.

EBs were dislodged from the microwells by pipetting media. Single cells were filtered from the suspension using a reversible strainer. EBs were resuspended in fresh neural induction media and then plated onto the prepared surface. Full media changes were performed until greater than 75% neural induction was observed, quantified visually by observed neural rosettes. Neural rosettes were selected using Neural Rosette Selection Reagent and dislodged by pipetting DMEM/F-12 into to the well. The suspension was centrifuged

at 350 g for 5 minutes to collect the rosettes. Neural rosettes were resuspended and plated onto a new coated well. A daily media change was performed henceforth until the cells obtained greater than 80% confluence, at which point they were frozen or passaged.

To passage cells, media was aspirated and 1 mL of 0.025% trypsin in DMEM was added to the well and incubated for 5 minutes. Cells were dislodged by pipetting and centrifuged at 300 g for 5 minutes. Cells were resuspended in neural progenitor media and plated on a PLO/laminin coated 6-well plate. Daily media changes were performed until the wells reached approximately 80% confluence.

To freeze cells were dissociated using the same protocol as passaging and centrifuged at 300 g for 5 minutes. The cell pellet was resuspended at 2–4x10^6 cells/mL in neural progenitor freezing medium. 1 mL of solution was placed in each cryovial. Cells were placed in a -80°C freezer overnight and then transferred into liquid nitrogen storage (-135°C).

3.2 Measuring polymerization and degradation time

Sample polymerization time was measured manually using a stopwatch. After mixing the timer was started and the sample was taken to have polymerized once it solidified.

Sample degradation time was observed visually. The sample was taken to be completely degraded once only fluid (no solid scaffold material) remained.

3.3 Scanning electron microscopy

Hydrogel samples were prepared for scanning electron microscopy (SEM) by either dehydration or freeze-drying.

Dehydration of the samples was performed with an ethanol series followed by application of hexamethyldisilazane (HDMS), a solution with a very low surface tension which hydrolyzes slowly allowing evaporation without disturbance of the gel structure. Ethanol and HDMS were obtained from Millipore-Sigma. Solutions of 30%, 70%, 90%, and 100% ethanol by volume were prepared in distilled, deionized water. A 1:10 sample to solution volume ratio was used; for example, 1 mL of hydrogel sample was suspended in 10 mL of ethanol solution. Each solution was left on the sample for 10 minutes in the fume hood and then aspirated and replaced by the next solution in the series. The 100% ethanol treatment was repeated twice, followed by the application of 50:50 ethanol/HDMS (v:v) for 10 minutes. 100% HDMS was then applied twice for 10 minutes and a third time to be left overnight in the fume hood. Samples were cut to size using a scalpel following dehydration and placed on sample stubs using double-sided tape.

For freeze drying samples were prepared in petri dishes and cut to size using a scalpel. These small samples were placed in the bottom of a 15 mL conical. Holes were punched in the lid of the conical and the sample was frozen overnight at -80°C. The conical was transferred to a jar and attached to a Leica CPD 300 critical point dryer overnight. After drying samples were placed onto stubs using double-sided tape.

SEM imaging was carried out using a Hitachi S-4800 FESEM at 1 kV accelerating voltage and a variety of magnifications.

3.4 Sample preparation for biological analysis

Pre-polymer and crosslinking solutions were prepared as described in section 3.3. Solutions were then moved into the biosafety cabinet (BSC). All solutions were filtered first with a 0.45 µm syringe filter to remove any large contaminants followed by a 0.2 µm syringe filter to remove smaller particles. The filtrate

was collected in a sterile conical. Additional bioink additives G, L, and P were filtered and added to either the pre-polymer or crosslinking solution.

NPCs were thawed and the cell pellet was collected by centrifuging at 300 g for 5 minutes. Cells were resuspended in the pre-polymer solution at a concentration of approximately $4x10^6$ cells/mL. 0.15 mL of the pre-polymer solution was deposited in 24-well cell culture plate, followed by 0.15 mL of crosslinking solution. This volume was previously optimized. Each sample formulation was prepared in triplicate. The plate was shaken to mix and the bioink allowed to set for up to 60 seconds. 0.5 mL of neural induction medium was added to each well.

A full media change was performed every second day until samples were degraded or used for analysis.

Table 1: Bioink formulations with their sample number, which base hydrogel was used, and what additives were present in the formulation. 0 represents no additive present, 1 represents the lowest concentration of additive used, and 1.5 represents a concentration 1.5x higher than the lowest used concentration.

Sample #	Hydrogel	Additive G	Additive L	Additive P
1	A	1	0	0
2	A	1.5	0	0
3	A and B	1	0	0
4	A and B	1.5	0	0
5	A	1	1	0
6	A	1.5	1	0
7	A and B	1	1	0
8	A and B	1.5	1	0
9	A	0	0	1
10	A and B	0	0	1
11	A	0	1	1
12	A and B	0	1	1

3.5 Flow cytometry

3.6.1 Preparation of cell suspension

Fixed bioink samples were transferred to the BSC and media was aspirated. 1 mL of 0.25% trypsin-EDTA (Life Technologies) was applied for up to 15 minutes to enzymatically dissolve the sample, mixing often with a pipette to promote dissolution. After samples were dissolved 1 mL of FBS was applied to quench the trypsin. Samples were transferred to 15 mL conicals and centrifuged at 300 g for 5 minutes to retrieve the cell pellet. Cells were resuspended and passed through a 60 µm reversible strainer to ensure a single cell suspension.

3.6.2 ViaCount assay

Cells were resuspended in 450 µL of ViaCount Reagent (Millipore Sigma) to obtain a final concentration less than $1x10^5$ cells/mL. Cells were allowed to stain for at least 5 minutes at room temperature, protected from light. A Guava EasyCyte HT flow cytometer and Guava-Soft EasyCyte software (Millipore) were used to read the stained cells and calculate the number of viable cells per mL, the percent viability, the total number of cells in the original sample given the original volume and the dilution factor.

3.6.2 Staining

Triplicates of the same formulation were combined into a single conical. Cells were collected by centrifuging at 300 g for 5 minutes. Cell pellets were resuspended in PBS and washed twice with 1 mL of

PBS, centrifuging at 300 g for 5 minutes between washes. Cell pellets were resuspended in 0.5 mL of flow cytometry fixation buffer (Millipore Sigma) and incubated at room temperature for 10 minutes, vortex mixing at minute 0 and 5. Cells were then washed twice with 1 mL of PBS and then resuspended in 1.5 mL flow cytometry permeabilization/wash buffer I (Millipore Sigma). 100 µL of solution was distributed into each well in a 96-well plate.

At day 7 samples were stained for TUJ-1, Olig2 and Nestin. At day 14 samples were stained for TUJ-1 and Olig2. Nestin was not stained for on day 14 because it was expected for the cells to lose their progenitor-like characterstics by this point. The antibodies and isotypes used are outlined in **Table 2**.

Table 2: Antibodies and isotypes used for flow cytometry.

Staining for	Name	Species	Production Company	Isotype Control
TUJ-1	Anti-beta-tubulin III antibody, clone TUJ1	Mouse anti-human	Stem Cell	Mouse IgG2a, kappa Isotype Control Antibody, Clone MOPC-173
Olig2	Anti-hOlig1,2,3	Mouse anti-human	R&D Systems	Mouse IgG_1 PE-conjugated Antibody
Nestin	Anti-hNestin	Mouse anti-human	R&D Systems	Mouse IgG_1 PE-conjugated Antibody

3 µL of antibody or antigen was added to each well (**Table A2, A3**). Wells were mixed thoroughly and covered with parafilm and foil then incubated at 4°C for 30 minutes. After 30 minutes they were mixed and incubated a further 30 minutes at 4°C. Plates were then centrifuged at 200g for 3 minutes. The supernatant was removed, and each well was washed and then resuspended in 100 µL permeabilization/wash buffer I.

3.6.3 Flow cytometry analysis

Data was collected with a Guava EasyCyte HT flow cytometer and Guava-Soft EasyCyte software (Millipore). Before beginning an experiment, the system was cleaned with bleach and guava instrument cleaning fluid and the waste vial was emptied. Gating was performed to exclude debris and gain controls were set for each isotype control such that fluorescence intensity above 10 was minimized. Each sample was collected up to a maximum of 5000 gated events.

3.6 Immunocytochemistry

Bioink samples were transferred to the benchtop and each well was fixed with 600 µL of 10% formalin (Millipore Sigma) at room temperature for 1 hour. Samples were then stained with 400 µL of primary antibody diluted in PBS (**Table 3**). Plates were wrapped in parafilm and foil and incubated at 4°C overnight. The following day each well was washed 3 times with 0.5 mL of PBS. Between each wash the plate was incubated at 4°C for 15 minutes. After the washes 400 µL of the secondary antibody diluted in PBS was added to each well. Plates were then wrapped in parafilm and foil and incubated at room temperature for 4 hours. Following incubation wells were washed 3 times with 0.5 mL PBS. Finally, 500 µL of DAPI at 0.105 µg/mL was added to each well. Plates were incubated for 3 minutes at room temperature and then wells were washed 3 times with 0.5 mL PBS prior to imaging. Samples were imaged using a Leica DMI3000B

inverted microscope, Lumen Dynamics X-Cite 120Q LED fluorescence light source, and QImaging camera and software.

Table 3: Primary antibodies and conjugates for ICC.

Staining for	Primary Antibody	Species	Dilution factor	Production Company	Conjugate	Dilution Factor
TUJ-1	Anti-beta-tubulin III antibody, clone TUJ1	Mouse	1:1000	Stem Cell	Alexa Fluor 488, Goat anti-mouse	1:500
DAPI	4',6-Diamidino-2-Phenylindole, Dihydrochloride	-	5 mg/mL	Life Technologies	-	-
NeuN	RBFOX3/NeuN Antibody	Rabbit	1:1000	Novus Biologicals	Alexa Fluor 647, Goat anti-rabbit	1:500
GFAP	Anti-GFAP antibody	Rabbit	1:1000	Stem Cell	Alexa Fluor 488, Goat anti-rabbit	1:500
TH	Anti-tyrosine hydroxylase antibody, clone TH-2	Mouse	1:1000	Stem Cell	Alexa Fluor 488, Goat anti-mouse	1:500

4.0 Results and Discussion

4.1 Optimizing additive G concentration

The concentration of additive G in the crosslinking solution was tested to maximize polymerization speed to create a bioink that was printable through a microfluidic system, where a gel state must be reached while the polymer is extruding to hold a complex shape. Low concentrations of additive G resulted in variable gelation times in the range of 5-13 seconds for formulations with hydrogel A and B and 10-14 seconds for formulations with only hydrogel A (**Figure 6**). These polymerization times are compatible with Aspect Biosystems microfluidic printer. It was concluded that the addition of hydrogel B led to a faster polymerization speed, which agrees with the literature. For both formulations additive G had no significant effect on polymerization speed. The highest concentration of additive G was used in further experiments.

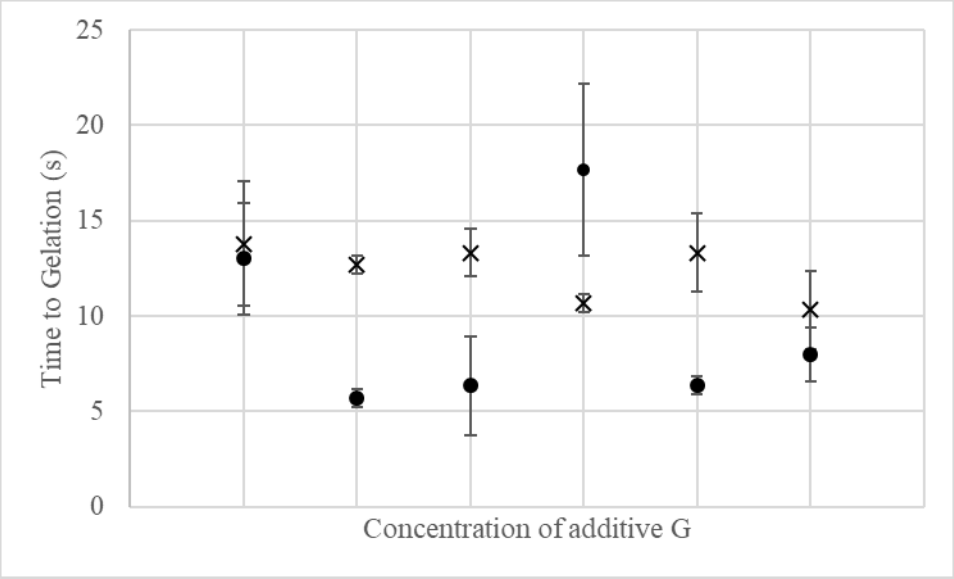

Figure 3: Polymerization speeds of bioinks with varying concentrations of additive G. The X markers indicate formulations with hydrogel A while the O markers indicate formulations with hydrogels A and B. N=3.

The concentration of additive G was then varied and the degradation of cell-seeded bioink samples was quantified. The highest concentration of additive G used in polymerization speed tests resulted in a time to degradation of approximately 11 days (**Figure 7**). Degradation was considered complete when the hydrogel had broken down and become fluid. Higher concentrations of additive G resulted in more desirable times to degradation of approximately 14 and 22 days. Since a desirable time to degradation is two weeks or greater the higher two additive G concentrations were used for further analysis. These concentrations will from now on be referred to as concentration 1 and 2 of additive G.

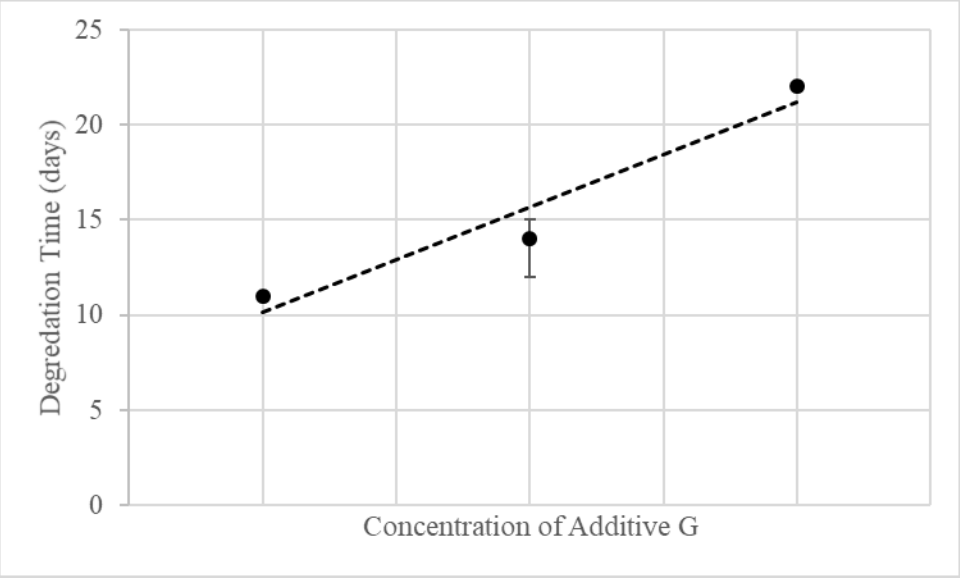

Figure 4: Average time of bioink degradation in days with increasing concentrations of additive G. Formulations with hydrogel A alone and hydrogels A and B degraded within two days of one another. N=2.

4.2 Characterizing mechanical properties

4.2.1 Scanning electron microscope imaging

Dehydrated bioink samples underwent extreme cracking. Cracking occurs when hydrogels are dried too quickly or with a solvent that has too much surface tension and the resulting images were disregarded since they did not represent accurate pore sizes. Freeze-drying samples resulted less damage to the samples but cracking still occurred. Even after 24 hours in a critical point dryer samples off-gassed slightly in the chamber resulting in some image contamination.

Pore sizes in the bioinks formulated with hydrogel A ranged from 0.07-4.2 µm based on manual measurement (**Figure 8-9**). Samples formulated with concentration 2 of additive G (**Figure 9**) displayed a more uniformly porous surface. Pore sizes in the bioinks formulated with hydrogels A and B exhibited much smaller pores, less than 0.5 µm in diameter, and much fewer pores permeated the surface (**Figure 10**). The addition of hydrogel B also appeared to reduce cracking, which is natural since it has a greater elastic modulus.

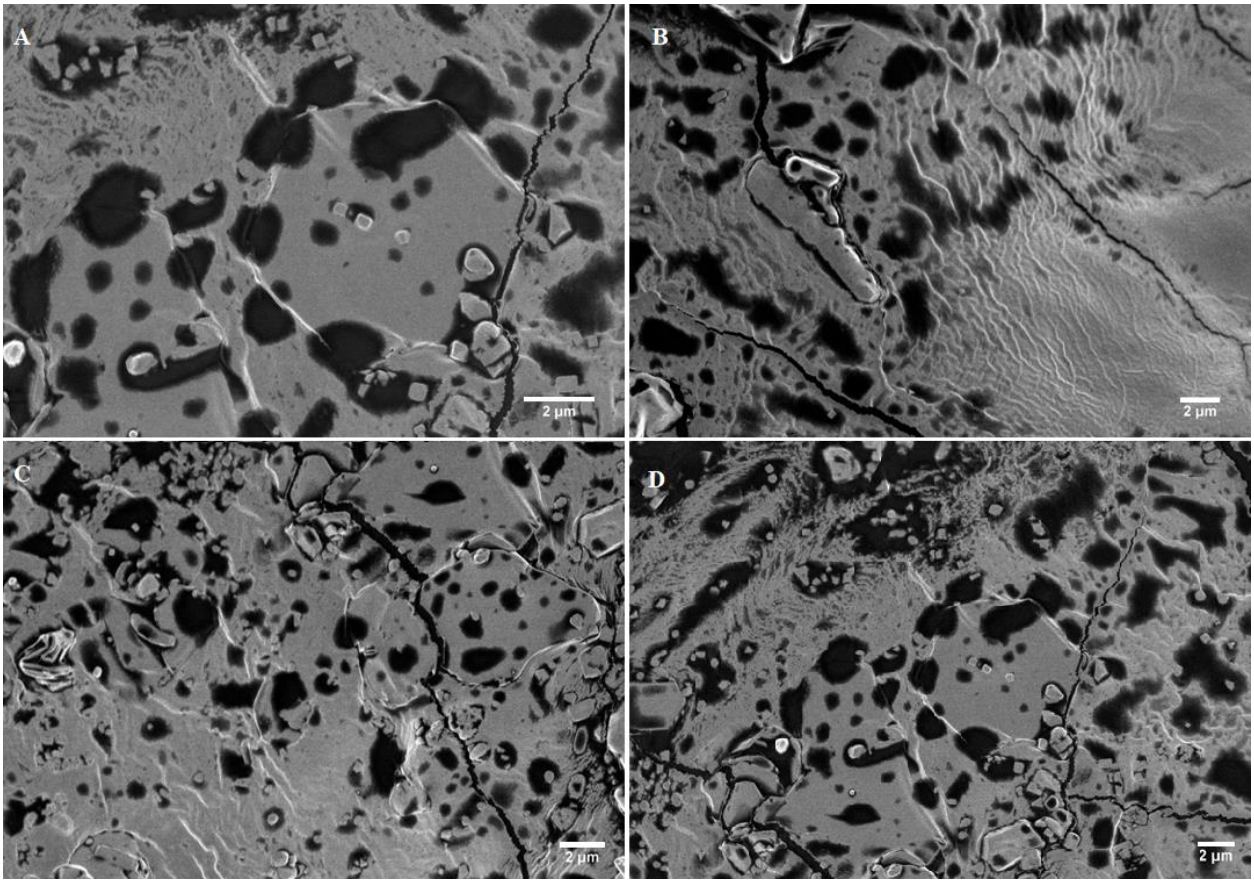

Figure 5: SEM images of hydrogel A bioink samples. (A-D) are different areas of a single sample made up of hydrogel and concentration 1 of additive G. Pores (dark holes) on the surface of this sample ranged from 0.07-4.2 µm in diameter based on manual measurement. Some cracking is visible on the surface of the sample due to tension while drying.

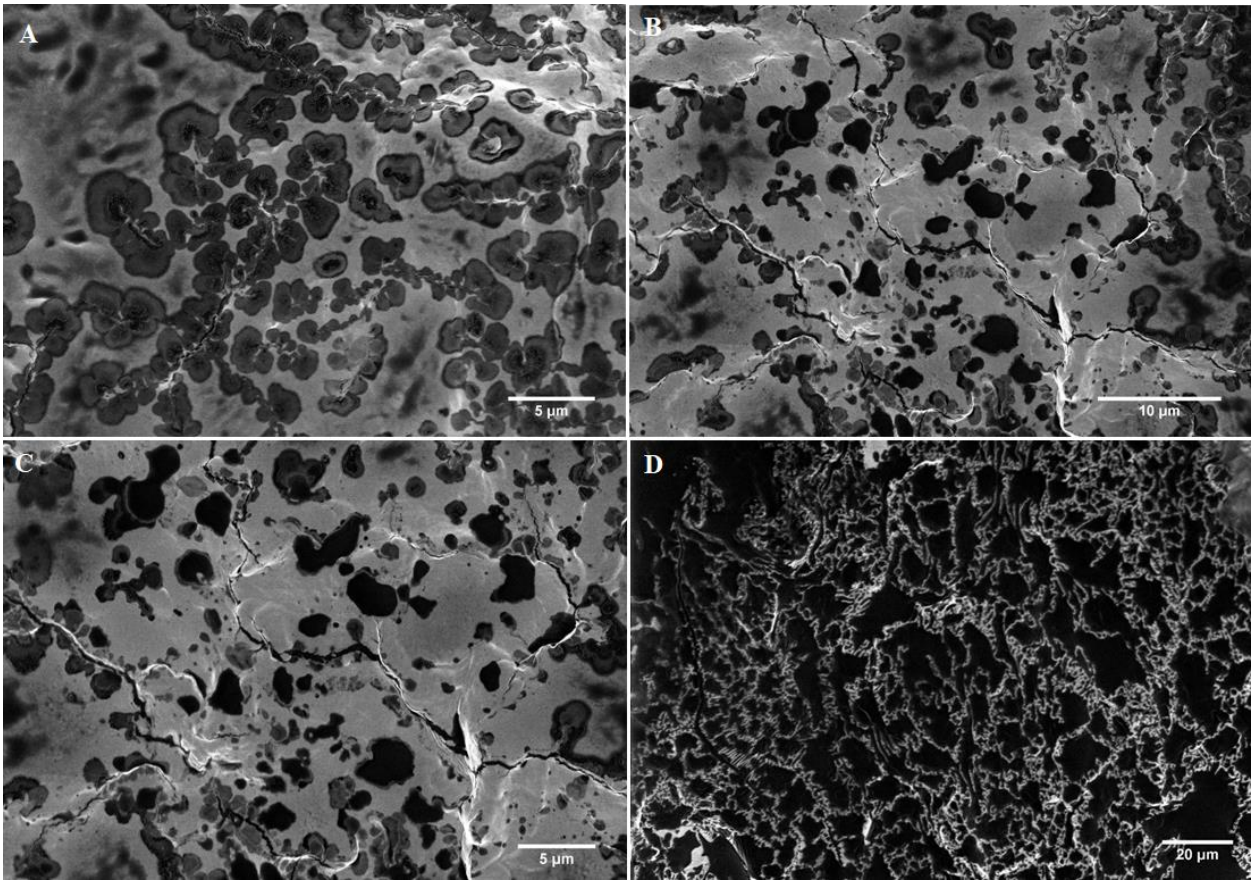

Figure 6: SEM images of bioink samples with hydrogel A. (A-D) are images of different area of the same sample made up with hydrogel A and concentration 2 of additive G. Pores (dark areas) on the surface of this sample ranged from 0.07-4.2 µm based on manual measurement. Again, some cracking is visible to due drying.

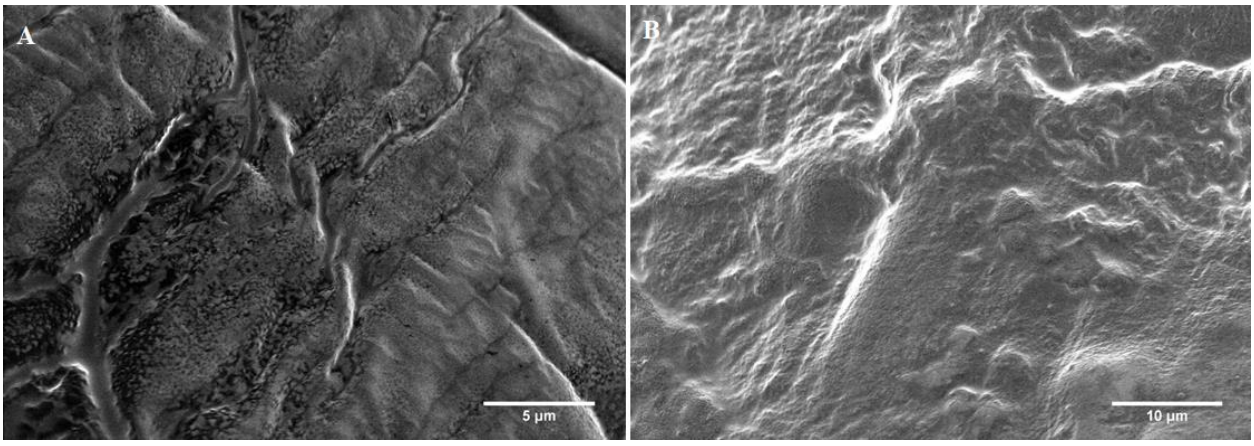

Figure 7: SEM images of bioink samples with hydrogels A and B. (A) is an image of the surface of a bioink formulated with concentration 1 of additive G, showing few surface pores with small diameters less than 0.5 µm. (B) is an image of the surface a bioink formulated with concentration 2 of additive G. No surface pores are visible in this image. In both (A) and (B) less cracking is observed in comparison to samples with only hydrogel A.

4.3 Biological analysis

A cell count was performed 24 hours after bioinks were prepared using the ViaCount Assay. Cell viability ranged from 35-99% in all formulations (**Figure 15**). No significant differences were found between formulations. It appears that the addition of hydrogel B decreases cell viability shortly after preparation, while the addition of additive L increases cell viability (**Figure 16**). Additives G and A had no effect on viability. This experiment should be repeated to verify these conjectures. On day 7 after preparation ICC was performed to view concentrations of DAPI, a nucleic marker, TUJ1, an early neuronal marker, and NeuN, a neural progenitor marker in cells seeded in the bioink samples. The presence of NeuN indicates that neural progenitors are still present within the bioink sample, while the presence of TUJ1 indicates that the neural progenitors have begun to differentiate into immature neurons. Formulation 1 (**Figure 17**) showed many cells were still positive for NeuN, indicating that they hadn't yet differentiated into immature neurons. Small clumps as in Figure 15(C) stained positive for TUJ1 indicating some differentiation. The addition of additive L appeared to increase neural differentiation (**Figure 18**). A greater expression of TUJ1 was seen in formulations which included additive L.

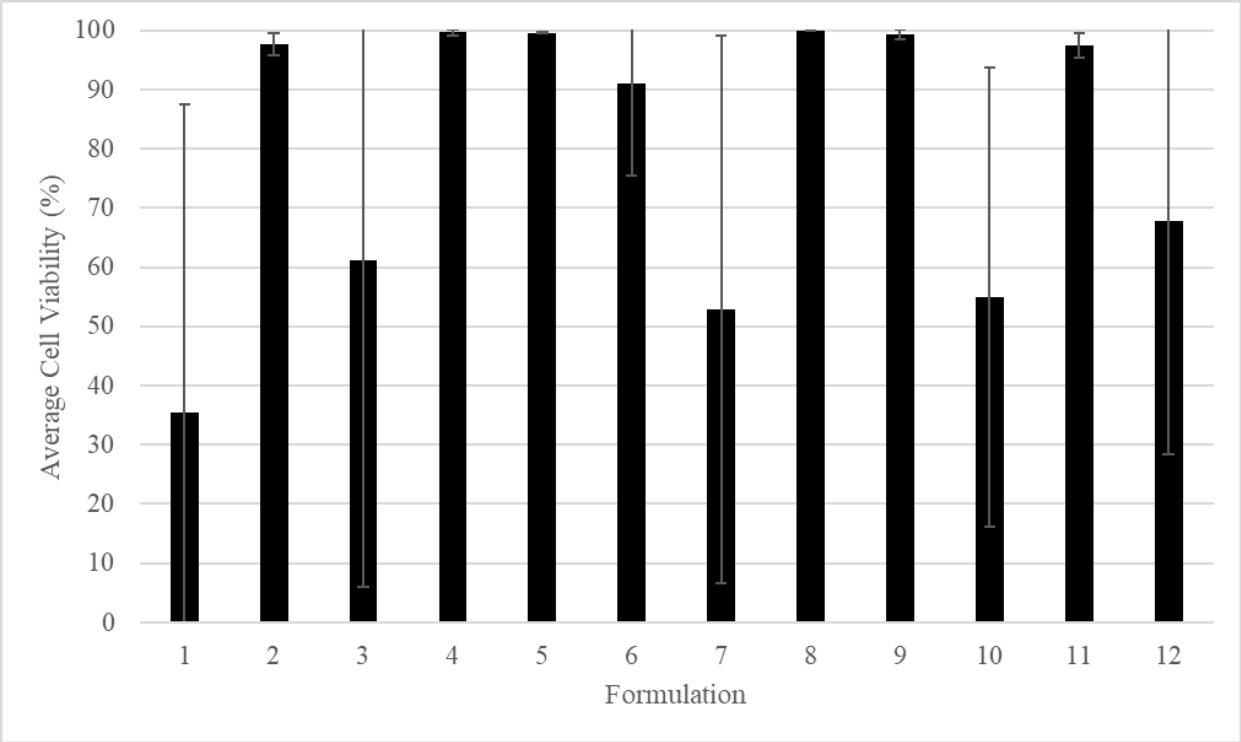

Figure 8: Cell viability 24 hours after preparation in each formulation (n=3). Viability ranged from 35-99%.

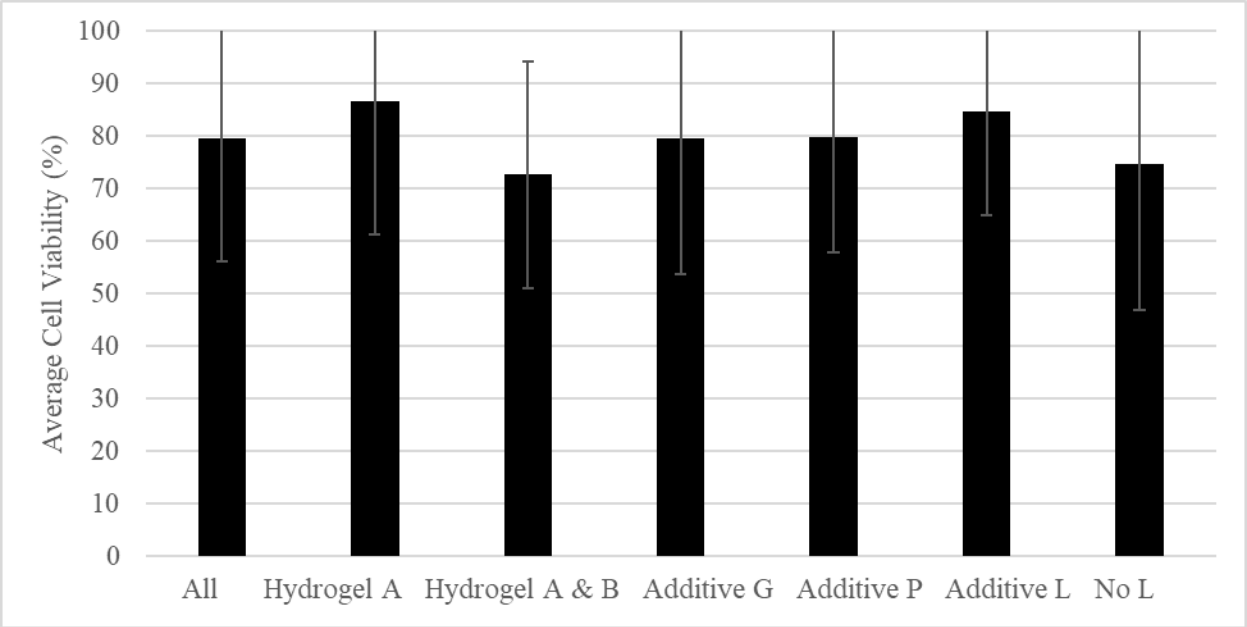

Figure 9: Cell viability 24 hours after preparation according to bioink constituents. No significant differences were found; however, the addition of hydrogel B appears to decrease cell viability while the addition of Additive L appears to increase cell viability. For each formulation n=3.

Bioink samples with hydrogel B contained live cells which nuclei stained positive for DAPI, but they expressed little NeuN or TUJ1, indicating that cells were not differentiating into neurons and that NPCs had perhaps died within the bioink.

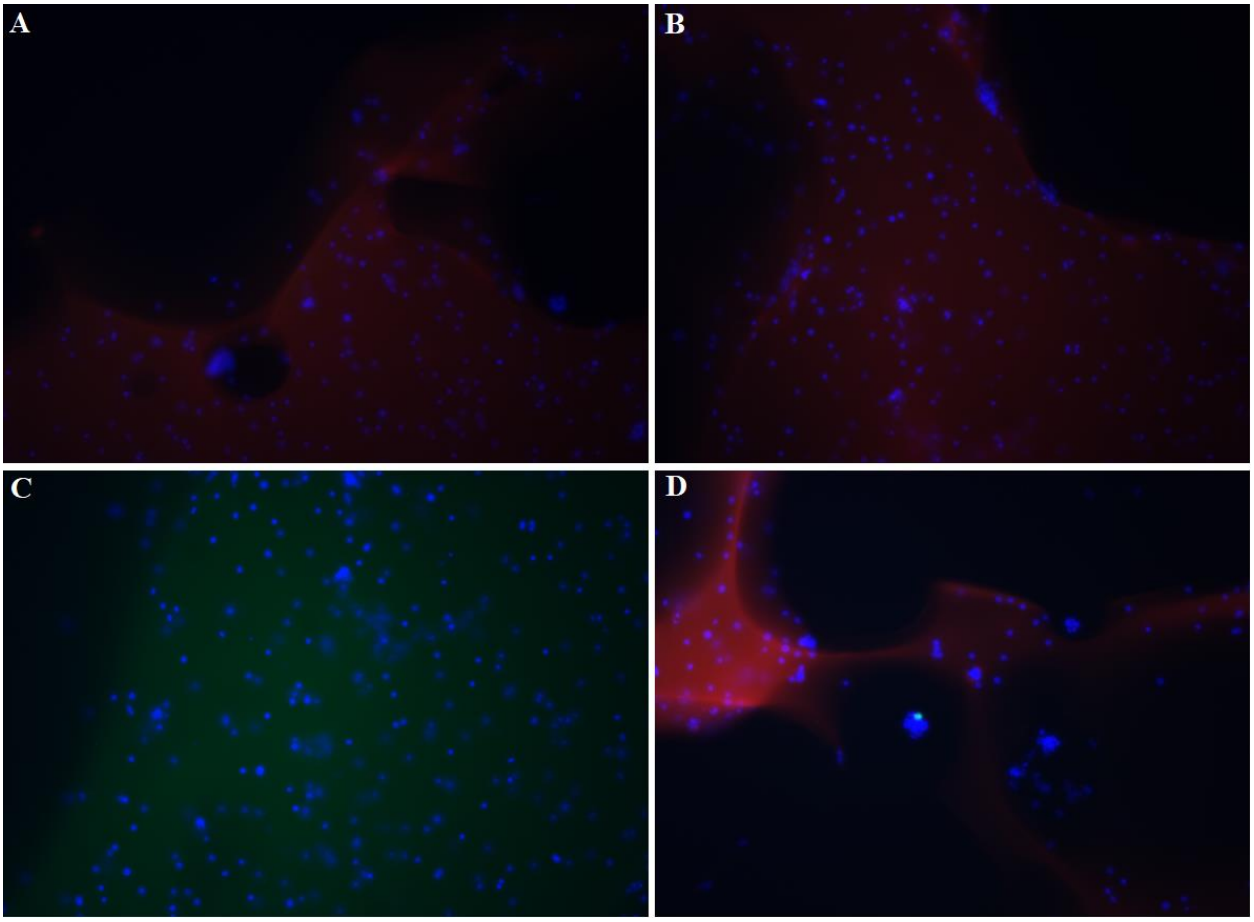

Figure 10: Samples of bioink formulation 1 (hydrogel A with concentration 1 of additive G) with nuclei stained with DAPI (blue), immature neurons stained for TUJ1 (green) and neural progenitors stained for NeuN (red). (A, B, and D) show clumps of neural progenitors expressing NeuN, while (D) shows a patch of cells which have begun to differentiate into immature neurons.

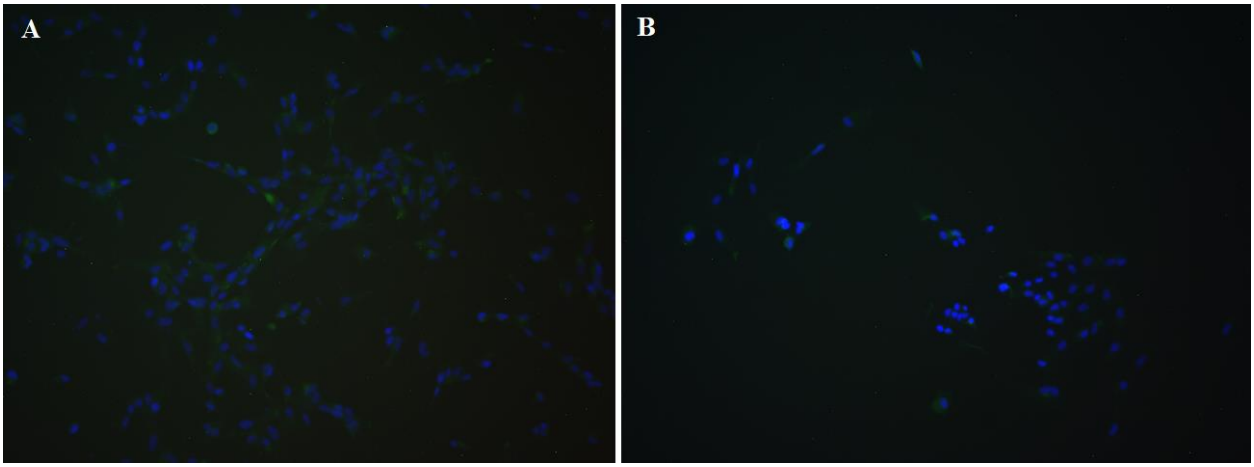

Figure 11: Samples of bioink formulation 5 (hydrogel A with concentration 1 of additive G and additive L) with nuclei stained with DAPI (blue), immature neurons stained with TUJ1 (green). Both (A) and (B) show clumps of cells which have begun to differentiate from neural progenitors into neurons.

Bioink samples were analyzed on Day 7 to quantify the cell population which were positive for TUJ1, an early neuronal marker, Nestin, a neural progenitor marker, and Olig2, which is present in both immature neurons and immature oligodendrocytes. Quantifying the percentage of cells positive for Nestin allows

quantifications of the number of cells which remain neural progenitors and have not yet developed. TUJ1 will indicate how many of the cells have begun differentiation into neurons while Olig2 can indicate if any of the cells will differentiate into oligodendrocytes instead. Several bioink samples contained too few live cells to give an accurate measurement (**Figure 17**) (**Table A4**). The addition of additive P appears to increase the percentage of cells with a neuronal fate as it increased the TUJ1 expression (**Figure 18**) (**Table A5**). All formulations are highly positive for Nestin which indicates that most cells are still in a progenitor-like state.

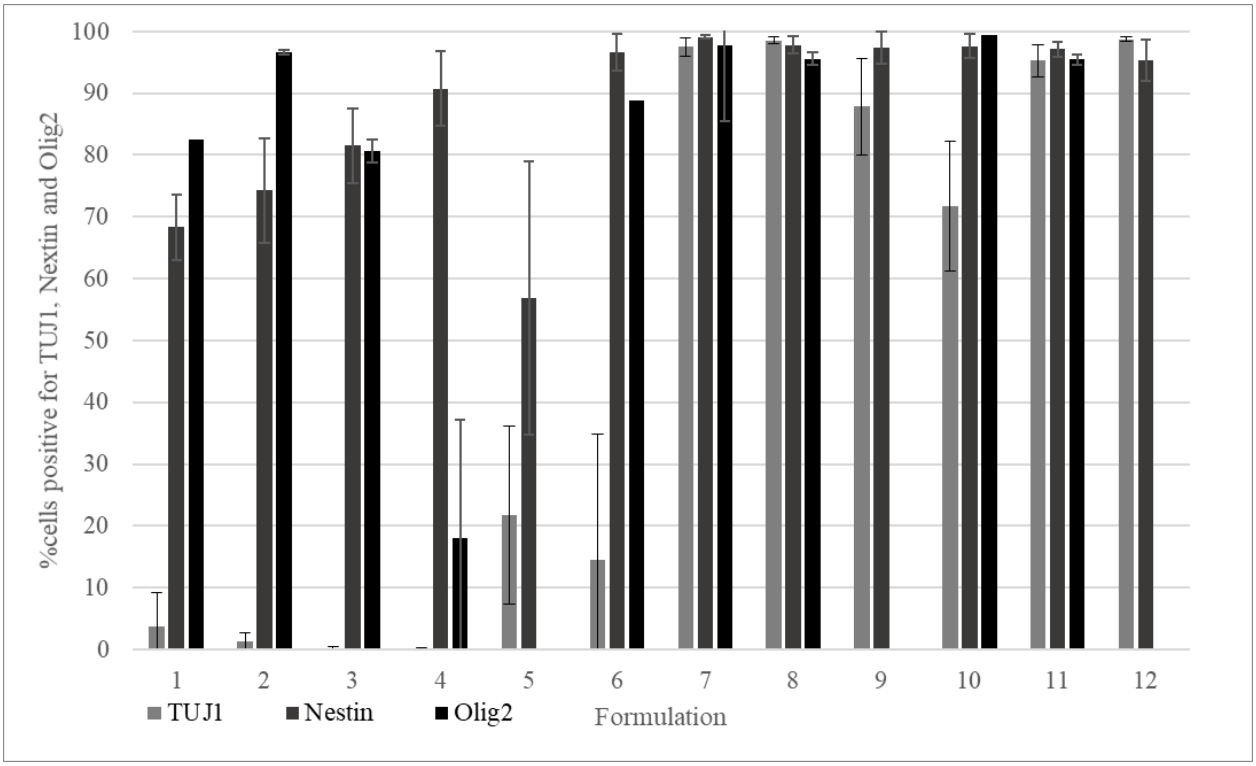

Figure 12: Percentage of cells positive for TUJ1 (indicating that they are differentiating into neurons), Nestin (indicating neural progenitors) and Olig2 (indicating immature neurons or oligodendrocytes) in each bioink formulation. The addition of additive P (formulations 9-12) appears to increase the percentage of cells with a neuronal fate. The high expression of Nestin across formulations indicates that many cells are still undifferentiated progenitors. Error bars represent 1 standard deviation. For each formulation n=3.

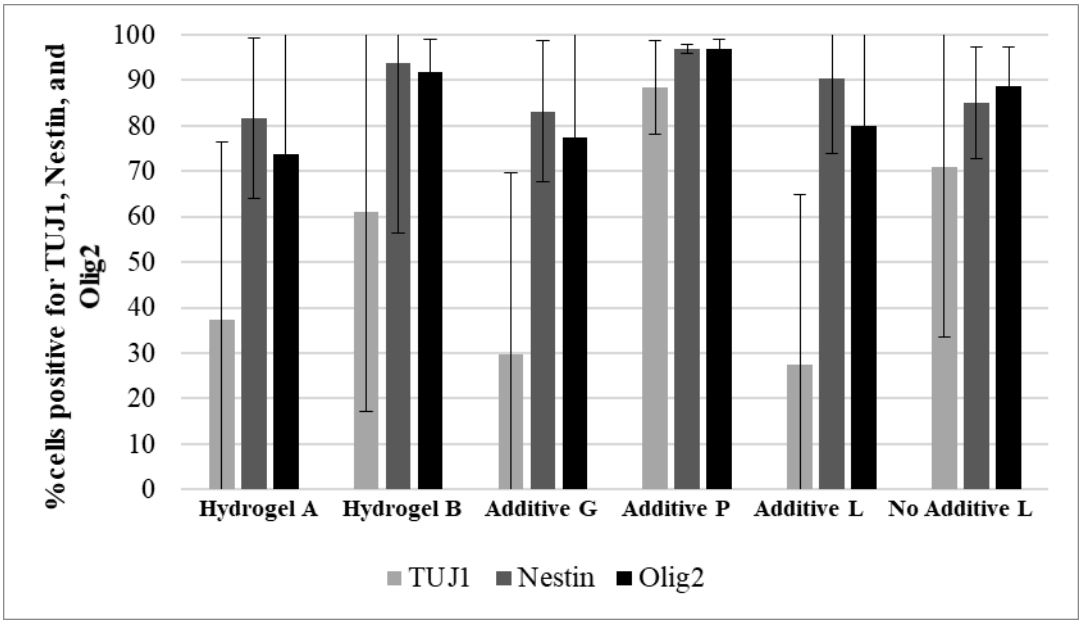

Figure 13: Percentage of cells positive for TUJ1 (indicating that they are differentiating into neurons), Nestin (indicating neural progenitors) and Olig2 (indicating immature neurons or oligodendrocytes) according to which additives were present. The addition of additive P appears to increase the percentage of cells with a neuronal fate. The high expression of Nestin across formulations indicates that many cells are still undifferentiated progenitors. Error bars represent 1 standard deviation. For each formulation n=3.

Bioink samples were imaged again 14 days after preparation to observe expression of DAPI, TUJ1, NeuN, and tyrosine hydroxylase (TH), a dopaminergic neuron marker. No formulations indicated the presence of dopaminergic neurons, however the increase of TUJ1 expression in all formulations indicates that more cells are differentiating into immature neurons. Hydrogel A formulations showed an increase in TUJ1 expression (**Figure 19**). Formulations with concentration 2 of additive G appeared to have extremely low expression of TUJ1, indicating that high concentrations of additive G may hinder neuronal differentiation. Formulations with hydrogel B similarly showed very low TUJ1 expression, therefore hydrogel B may have a negative effect on neuronal differentiation (**Figure 20**).

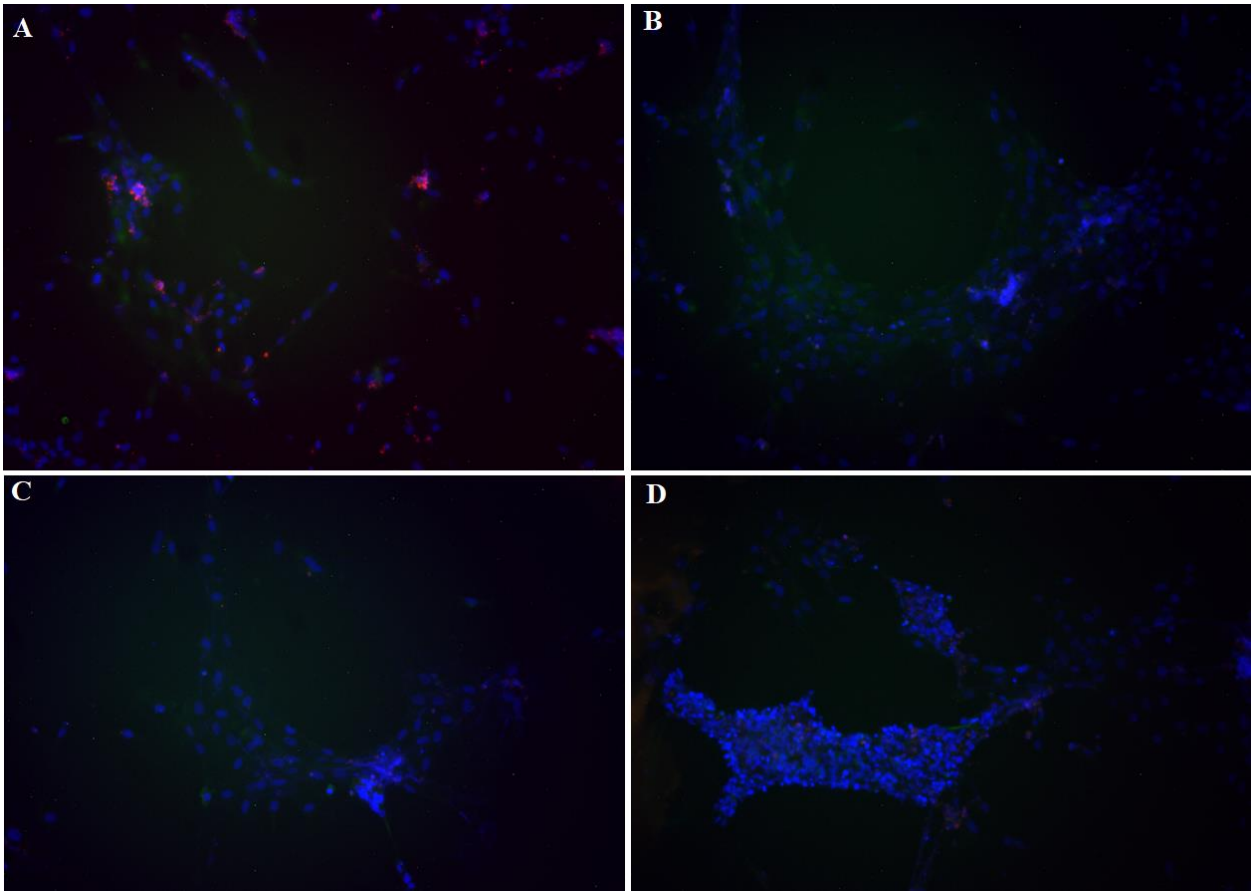

Figure 14: Cells 14 days after preparation in hydrogel A with concentration 1 of additive G (A, B) and hydrogel A with concentration 2 of additive G (C, D). Formulations show an increased expression of TUJ1 (green) and a decreased expression of NeuN (red), indicating that neural progenitors are differentiating into neurons. DAPI (blue) indicates cell nuclei.

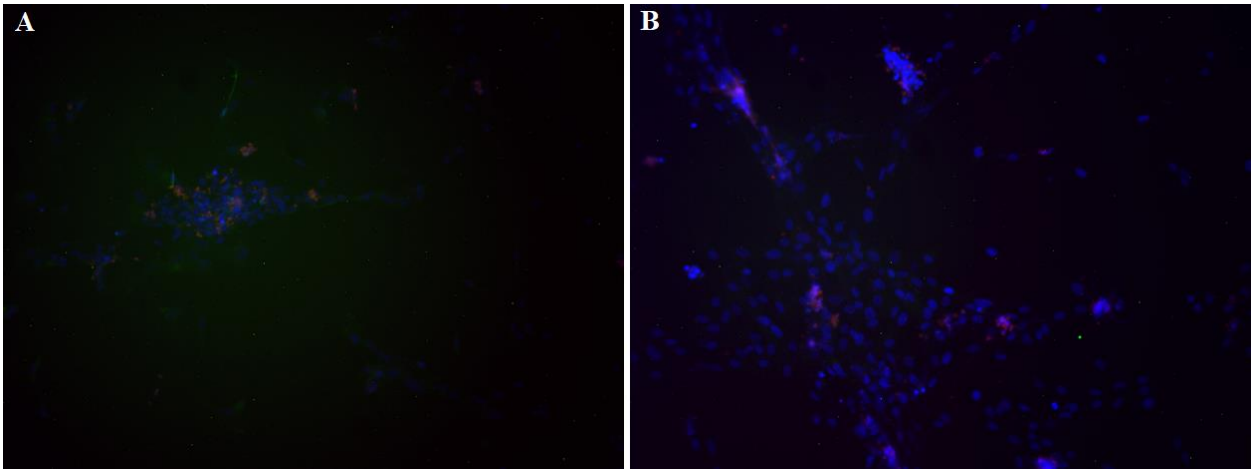

Figure 15: Cells 14 days after preparation stained for TUJ1 (green), NeuN (red) and DAPI (blue). (A) is formulation 9 with hydrogel A and additive P while (B) is formulation 10 with hydrogels A and B and additive P. It appears that hydrogel B decreases the expression of TUJ1 and therefore decreases the number of cells which differentiate into neurons.

5.0 Conclusion and future work

Current methods of engineering neural tissue are limited due to the time-consuming, hands-on nature of 2-D hiPSC differentiation protocols. Bioprinting could be the basis of a sterile, high-throughput method of engineering physiologically relevant neural tissue constructs for disease modelling and drug discovery. The field is currently limited by the transfer of microfluidic systems into biologically relevant applications and the development of cytocompatible and printable bioinks.

The proposed bioink formulations retain a high cell viability shortly after polymerization as well as a high cell viability and TUJ1 expression after two weeks in culture, indicating that they can support the differentiation of hiPSC-derived NPCs into mature neurons through the polymerization and into longer time periods. The addition of hydrogel B appears to decrease the percentage of cells destined for a neuronal fate. The addition of additive L appears to increase cell viability shortly after printing. The addition of additives G and P do not seem to affect cell differentiation. It is recommended that future studies focus on bioinks derived from hydrogel A with the addition of additive L and either additive G or P.

In future work it is recommended that SEM imaging be performed in a biological SEM, where a low vacuum is applied, and full sample dehydration is not necessary. This would remove the risk of sample cracking and degradation due to dehydration and/or freeze-drying. It is recommended that cell suspensions be filtered prior to resuspended for flow cytometry analysis. Degradation of the bioink was incomplete in some cases and intact pieces of the hydrogel may affect results. It is further recommended that 3 and 4-week experiments be performed on the recommended bioink formulation to characterize the mature neurons which develop in terms of cell type (dopaminergic, cholinergic, etc.) and electrophysiology.

6.0 Conflict of interest

The author declares that the research was conducted in the absence of any commercial or financial relationships that could be construed as a potential conflict of interest.

7.0 Funding

This work was supported by the Stem Cell Network Commercialization Impact Grant program along with funding the Natural Science and Engineering Research Council Discovery Grants program and the Canada Research Chair program.

8.0 References

[1] Institute for Neurodegenerative Diseases, "The Cost of Dementia," 13 July 2017. [Online]. Available: https://ind.ucsf.edu/supporting-our-work/cost-dementia.

[2] M. Vila and S. Przedborksi, "Targeting programmed cell death in neurodegenerative diseases," *Nature Reviews Neuroscience,* pp. 365-375, 2003.

[3] M. Levy, N. Boulis, M. Rao and C. N. Svendsen, "Regenerative cellular therapies for neurologic diseases," *Brain Research,* pp. 88-96, 2016.

[4] A. Dove, "Cell-based therapies go live," *Nature Biotechnology,* pp. 339-343, 2002.

[5] R. Y Tam, T. Fuehrmann, N. Mitrousis and M. S. Shoichet, "Regenerative Therapies for Central Nervous System Diseases: A Biomaterials Approach," *Neuropsychopharmacology,* vol. 39, pp. 169-188, 169-188 2014.

[6] M. Tsintou, K. Dalamagkas and A. Seifalian, "Advances in regenerative therapies for spinal cord injury: a biomaterials approach," *Neural Regeneration Research,* vol. 10, no. 5, pp. 726-42, 2015.

[7] M. Cooke, K. Vulic and M. Shoichet, "Design of biomaterials to enhance stem cell survival when transplanted into the damaged central nervous system," *Soft Matter,* pp. 4988-4998, 2010.

[8] F. Rossi and E. Cattaneo, "Neural stem cell therapy for neurological diseases: dreams and reality," *Nature Reviews Neuroscience,* pp. 401-409, 2002.

[9] L. A. Struzyna, K. Katiyar and D. K. Cullen, "Living scaffolds for neuroregeneration," *Current Opinion in Solid State and Materials Science,* pp. 308-318, 2014.

[10] A. Skardal and A. Atala, "Biomaterials for Integration with 3-D Bioprinting," *Annals of Biomedical Engineering,* pp. 730-746, 2015.

[11] L. E. Freed, G. Vunjak-Novakovic, R. J. Biron, D. B. Eagles, D. C. Lesnoy, S. K. Barlow and R. Langer, "Biodegradable Polymer Scaffolds for Tissue Engineering," *Nature Biotechnology,* pp. 689-693, 1994.

[12] A. J. Mothe and C. H. Tator, "Advances in stem cell therapy for spinal cord injury," *The Journal of Clinical Investigation,* pp. 3824-3834, 2012.

[13] J. Itskovitz-Eldor, M. Schuldiner, D. Karsenti, A. Eden, O. Yanuka, M. Amit, H. Soreg and N. Benvenisty, "Differentiation of human embryonic stem cells into embryoid bodies comprising the three embryonic germ layers," *Molecular Medicine,* pp. 88-95, 2000.

[14] M. Bobbert, "Ethical questions concerning research on human embryos, embryonic stem cells and chimeras," *Biotechnology Journal,* pp. 1352-1369, 2006.

[15] K. Takahashi, K. Tanabe, M. Ohnuki and e. al., "Induction of pluripotent stem cells from adult human fibroblasts by defined factors," *Cell,* vol. 131, no. 5, pp. 861-72, 2007.

[16] H. Kamao, M. Mandai, S. Okamato, N. Sakai, A. Suga, S. Sugita, J. Kiryu and M. Takahashi, "Characterization of Human Induced Pluripotent Stem Cell-Derived Retinal Pigment Epithelium Cell Sheets Aiming for Clinical Application," *Stem Cell Reports,* pp. 205-218, 2014.

[17] S. Durnaoglu, S. Genc and K. Genc, "Patient-Specific Pluripotent Stem Cells in Neurological Diseases," *Stem Cells International,* p. doi:10.4061/2011/212487, 2011.

[18] S. V. Murphy and A. Atala, "3D bioprinting of tissues and organs," *Nature Biotechnology,* pp. 773-785, 2014.

[19] M. A. McMahon, M. Rahdar and M. Porteus, "Gene editing: not just for translation anymore," *Nature Methods,* pp. 28-31, 2012.

[20] U. Freudenberg, A. Hermann, P. B. Welzel, K. Stirl, S. C. Schwarz, M. Grimmer, A. Zieris, W. Panyanuwat, S. Zschoche and D. Meinhold, "A star-PEG-heparin hydrogel platform to aid cell replacement therapies for neurodegenerative diseases," *Biomaterials,* pp. 5049-5060, 2008.

[21] C. Gardin, V. Vindigni, E. Bressan, L. Ferroni, E. Nalesso, A. Della Puppa, D. D'Avella, D. Lops, P. Pinton and B. Zavan, "Haluronan and Fibrin Biomaterials as Scaffolds for Neuronal Differentiation of Adult Stem Cells Derived from Adipose Tissue and Skin," *International Journal of Molecular Science,* pp. 6749-6764, 2011.

[22] R. A. Perez, S.-J. Choi, C.-M. Han, J.-J. Kim, H. Shim, K. W. Leong and H.-W. Kim, "Biomaterials control of pluripotent stem cell fate for regenerative therapy," *Progress in Materials Science,* pp. 234-293, 2016.

[23] P. J. Johnson, A. Tatara, A. Shiu and S. E. Sakiyama-Elbert, "Controlled Release of Neurotrophin-3 and Platelet-Derived Growth Factor From Fibrin Scaffolds Containing Neural Progenitor Cells Enhances Survival and Differentiation Into Neurons in a Subacute Model of SCI," *Cell Transplantation,* vol. 19, no. 1, pp. 89-101, 2010.

[24] T. S. Wilems, J. Pardieck, N. Iyer and S. E. Sakiyama-Elbert, "Combination Therapy of Stem Cell Derived Neural Progenitors and Drug Delivery of Anti-Inhibitory Molecules for Spinal Cord Injury," *Acta Biomateriala,* pp. 23-32, 2015.

[25] H. Itosaka, S. Kuroda, H. Shichinohe, H. Yasuda, S. Yano, K. Shintaro, R. Kawamura, H. Hida and Y. Iwasaki, "Fibrin Matrix Provides a Suitable Scaffold for Bone Marrow Stromal Cells Transplanted into Injured Spinal Cord: A Novel Material for CNS Tissue Engineering," *Neuropathology,* pp. 248-57, 2009.

[26] P. Lu, Y. Wang, L. Graham, K. McHale, M. Gao, D. Wu and J. Brock, "Long-Distance Growth and Connectivity of Neural Stem Cells after Severe Spinal Cord Injury," *Cell,* pp. 1264-1273, 2012.

[27] P. Elias and M. Spector, "Implantation of a Collagen Scaffold Seeded with Adult Rat Hippocampal Progenitors in a Rat Model of Penetrating Brain Injury," *Journal of Neuroscience Methods,* pp. 199-211, 2012.

[28] C. C. Tate, D. A. Shear, M. C. Tate, D. R. Archer, D. G. Stein and M. C. LaPlaca, "Laminin and Fibronectin Scaffolds Enhance Neural Stem Cell Transplantation into the Injured Brain," *Journal of Tissue Engineering and Regenerative Medicine,* pp. 208-217, 2009.

[29] E. Sykova, P. Jendelova and L. Urdzikova, "Bone Marrow Stem Cells and Polymer Hydrogels - Two Strategies for Spinal Cord Injury Repair," *Cellular and Molecular Neurobiology,* pp. 111-127, 2006.

[30] A. M. Hopkins, E. DeSimone, K. Chwalek and D. L. Kaplan, "3D in vitro modeling of the central nervous system," *Progress in Neurobiology,* pp. 1-25, 2015.

[31] Y. Shao, J. Sang and J. Fu, "On human pluripotent stem cell control: The rise of 3D bioengineering and mechanobiology," *Biomaterials,* vol. 52, pp. 26-43, 2015.

[32] S. M. Chambers, C. A. Fasana, E. P. Papapetrou, M. Tomishima, M. Sadelain and L. Studer, "Highly efficient neural conversion of human ES and iPS cells by dual inhibition of SMAd signaling," *Nature Biotechnology,* pp. 275-280, 2009.

[33] E. Lippmann, M. Estevez-Silva and R. Ashton, "Defined human pluripotent stem cell culture enables highly efficient neuroepithelium derivation without small molecule inhibitors," *Stem Cells,* vol. 32, no. 4, pp. 1032-1042, 2014.

[34] J. Edgar, M. Robinson and S. Willerth, "PBS," *Acta Biomaterialia,* vol. 51, pp. 237-245, 2017.

[35] M. T. Ahmad and N. Makoto, "Three-dimensional Bioprinting: Toward the Era of Manufacturing Human Organs as Spare Parts for Healthcare and Medicine," *Tissue Engineering Part B: Reviews,* vol. 23, no. 13, pp. 245-256, 2017.

[36] M. Robinson, S.-y. Yau, L. Sun, N. Gabers, E. Bibault, B. R. Christie and S. M. Willerth, "Optimizing Differentiation Protocols for Producing Domapinergic Neurons from Human Induced Pluripotent Stem Cells for Tissue Engineering Applications," University of Victoria Engineering Faculty Publications, Victoria, 2016.

[37] Q. Gu, E. Tomaskovic-Crook, R. Lazano, Y. Chen, R. M. Kapsa, Q. Zhou, G. G. Wallace and J. M. Crook, "Functional 3D Neural Mini-Tissues from Printed Gel-Based Bioink and Human Neural Stem Cells," *Advanced Healthcare materials,* vol. 5, no. 12, pp. 1429-1438, 2016.

[38] M. P. Schwartz, Z. Hou, N. E. Propson, J. Zhang, C. J. Engstrom, V. Santos Costa, P. Jiang, B. K. Nguyen, J. M. Bolin, W. Daly, Y. Wang, R. Stewart, C. D. Page, W. L. Murphey, Thomson and J. A, "Human pluripotent stem cell-derived neural constructs for predicting neural toxicity," *Proceedings of the National Acedmy of Sciences of the United States of America,* vol. 112, no. 40, pp. 12516-12521, 2015.

[39] C. O'Brien, B. Holmes, S. Faucett and L. Zhang, "Three-dimensional printing of nanomaterial scaffolds for complex tissue regeneration," *Tissue Engineering Part B,* vol. 21, no. 1, pp. 103-14, 2015.

[40] S. Willerth, K. Arendas, D. Gottlieb and S. Sakiyama-Elbert, "Optimization of fibrin scaffolds for differentiation of murine embryonic stem cells into neural lineage cells," *Biomaterials,* pp. 5990-6003, 2006.

[41] S. Willerth, P. Johnson, D. Maxwell, S. Parsons, M. Doukas and S. Sakiyama-Elbert, "Rationally designed peptides for controlled release of nerve growth factor from fibrin matrices," *Journal of Biomedical Materials Research Part A,* pp. 13-23, 2007.

[42] S. Willerth, T. Faxel, D. Gottlieb and S. Sakiyama-Elbert, "The efects of soluble growth factors on embryonic stem cell differentiation inside of fibrin scaffolds," *Stem Cells,* pp. 2235-2244, 2007.

[43] S. Willerth, A. Rader and S. Sakiyama-Elbert, "The effects of controlled growth factor release on embryonic stem cell differentiation inside of fibrin scaffolds," *Stem Cell Research,* pp. 205-218, 2008.

[44] K. Kolehmainen and S. Willerth, "Preparation of 3D Fibrin Scaffolds for Stem Cell Culture Applications," *Journal of Visualized Experiments: Bioengineering,* 2012.

[45] A. Montgomery, A. Wong, N. Gabers and S. Willerth, "Engineering personalized neural tissue by combining induced pluripotent stem cells with fibrin scaffolds," *Biomaterials Science,* pp. 401-403, 2015.

[46] R. Lozano, L. Stevens, B. C. Thompson, K. J. Gilmore, R. Gorkin, E. M. Stewart, M. in het Panhuis, M. Romero-Ortega and G. G. Wallace, "3D printing of layered brain-like structures using peptide modified gellan gum substrates," *Biomaterials,* vol. 67, pp. 264-273, 2015.

[47] R. Pittier, F. Sauthier, J. Hubbell and H. Hall, "Neurite extension and in vitro myelination within three-dimensional modified fibrin matrices," *Journal of Neurobiology,* vol. 63, no. 1, pp. 1-14, 2005.

[48] S. R. Caliari and J. A. Burdick, "A practical guide to hydrogels for cell culture," *Nature Methods,* pp. 405-414, 2016.

[49] J. K. Carrow, P. Kerativitayanan, M. K. Jaiswal, G. Lokhande and A. Caharwar, "Polymers for Bioprinting," in *Essentials of 3D Biofabrication and Translation,* Elsevier Inc, 2015, pp. 229-248.

[50] Y. Wang, Y. M. Kim and R. Langer, "In vivo degradation characteristics of poly(glycerol sebacate)," *Journal of Biomedical Materials Research Part A,* vol. 66A, no. 1, pp. 192-197, 2003.

[51] J. Anderson and J. Jones, "Phenotypic dichotomies in the foreign body reaction.," *Biomaterials,* vol. 28, pp. 5114-5120, 2007.

[52] J. Anderson, A. Rodriguez and D. Chang, "Foreign body reaction to biomaterials," *Seminars in Immunology,* vol. 20, pp. 86-100, 2007.

[53] H. N. Chia and B. M. Wu, "Recent advances in 3D printing of biomaterials," *Journal of Biological Engineering,* pp. DOI 10.1186/s13036-015-0001-4, 2015.

[54] B. C. Gross, J. L. Erkal, S. Y. Lockwood, C. Chen and D. M. Spence, "Evaluation of 3D Printing and Its Potential Impact on Biotechnology and the Chemical Sciences," *Analytical Chemistry*, pp. 3240-3253, 2014.

[55] A. Pfister, R. Landers, A. Laib, U. Hubner, R. Schmelzeisen and R. Mulhaupt, "Biofunctional rapid prototyping for tissue-engineering applications: 3D bioplotting versus 3D printing," *Journal of Polymer Science Part A: Polymer Chemistry*, pp. 624-638, 2004.

[56] S. M. Potter and T. B. DeMarse, "A new approach to neural cell culture for long-term studies," *Journal of Neuroscience Methods*, pp. 17-24, 2001.

[57] Q. Gu, E. Tomaskovic-Crook, R. Lazono, Y. Chen, R. Kapsa, Q. Zhou and e. al, "Functional 3D neural mini-tissues from printed gel-based bioink and human neural stem cells," *Advanced Healthcare Materials*, vol. 5, pp. 1429-1438, 2016.

[58] Y.-B. Lee, S. Polio, W. Lee, G. Dai, L. Menon, R. S. Carroll and S.-S. Yoo, "Bio-printing of collagen and VEGF-releasing fibrin gel scaffolds for neural stem cell culture," *Experimental Neurology*, vol. 223, no. 2, pp. 645-652, 2010.

[59] Stem Cell Technologies, "Generation and Culture of Neural Progenitor Cells using the STEMdiff Neural System," Stem Cell Technologies, 2017.

[60] G.-h. Cui, S.-j. Shao, J.-j. Yang, J.-r. Liu and H.-d. Guo, "Designer Self-Assemble Peptides Maximize the Therapeutic Benefits of Neural Stem Cell Transplantation for Alzheimer's Disease via Enhancing Neuron Differentiation and Paracrine Action," *Molecular Neurobiology*, pp. 1108-1123, 2016.

[61] M. A. Lancaster, M. Renner, C.-A. Martin, D. Wenzel, L. S. Bicknell, M. E. Hurles, T. Homfray, J. M. Penninger, A. P. Jackson and J. A. Knoblich, "Cerebral organoids model human brain development and microcephaly," *Nature*, vol. 501, pp. 373-379, 2013.

[62] H. S. Rafat, O. Yoshikazu and R. K. Puri, "Current Status and Challenges of Three-Dimensional Modeling and Printing of Tissues and Organs," *Tissue Engineering Part A*, vol. 23, no. 11-12, pp. 471-473, 2017.

[63] E. Hoch, G. E. Tovar and K. Borchers, "Bioprinting of artificial blood vessels: current approaches towards a demanding goal," *European Journal of Cardio-Thoracic Surgery*, pp. 767-778, 2014.

[64] S. J. Hollister, "Porous scaffold design for tissue engineering," *Nature Materials*, pp. 518-524, 2006.

[65] K. Tan, C. Chua, K. Leong, C. Cheah, W. Gui, W. Tan and F. Wiria, "Selective laser sintering of biocompatible polymers for applications in tissue engineering," *BioMedical Materials and Engineering*, pp. 113-124, 2005.

[66] C. Chua, K. Leong, K. Tan, F. Wiria and C. Cheah, "Development of tissue scaffolds using selective laser sintering of polyvinyl alcohol/hydroxyapatite biocomposite for craniofacial and joint defects," *Journal of Materials Science: Materials in Medicine*, pp. 1113-1121, 2004.

[67] T. Xu, C. A. Gregory, P. Molnar, X. Cui, S. Jalota, S. B. Bhaduri and T. Boland, "Viability and electrophysiology of neural cell structures generated by the inkjet printing method," *Biomaterials,* vol. 27, no. 19, pp. 3580-3588, 2006.

[68] B. Lorber, W.-K. Hsiao, I. M. Hutchings and K. R. Martin, "Adult rat retinal ganglion cells and glia can be printed by piezoelectric inkjet printing," *Biofabrication,* 2014.

[69] S. Suri, L.-H. Han, W. Zhang, A. Singh, S. Chen and C. E. Schmidt, "Solid freeform fabrication of designer scaffold of hyaluronic acid for nerve tissue engineering," *Biomedical Microdevices,* vol. 13, no. 6, pp. 983-993, 2011.

[70] J. Curley, S. Jennings and M. Moore, "Fabrication of micropatterened hydrogels for neural culture systems using dynamic mask projection photolithography," *Journal of Visualized Experiments,* vol. 48, p. 2636, 2011.

[71] S.-J. Lee, M. Nowicki, B. Harris and L. G. Zhang, "Fabrication of a Highly Aligned Neural Scaffold via a Table Top Stereolithography 3D Printing and Electrospinning," *Tissue Engineering: Part A,* vol. 23, no. 11-12, pp. 491-502, 2017.

[72] W. Zhu, J. K. George, V. J. Sorger and L. G. Zhang, "3D printing scaffold coupled with low level light therapy for neural tissue regeneration," *Biofabrication,* vol. 9, no. 2, 2017.

[73] F.-Y. Hsieh, H.-H. Lin and S.-h. Hsu, "3D bioprinting of neural stem cell-laden thermoresponsive biodegradable polyurethane hydrogel and potential in central nervous system repair," *Biomaterials,* vol. 71, pp. 48-57, 2015.

[74] S. U. Kim and J. de Villis, "Stem Cell-Based Therapy in Neurological Diseases: A Review," *Journal of Neuroscience Research,* vol. 87, pp. 2183-2200, 2009.

9.0 Appendix 1

Table A 1: Bioprinting neural tissue in vitro by a variety of printing methods using different cell types.

Bioink	Cell type	Cell Source	Printing method	Outcome	References
Alginate, carboxy-methyl chitosan, agarose	Cortical neural stem cells encapsulated in the scaffold	Human	Micro extrusion bioprinting	Proliferated for 10 days with spontaneous activity and a bicuculline-induced increase calcium response, predominantly expressing gamma-aminobutyric acid	[37]
Collagen and fibrin, fibrin loaded with VEGF	Neural stem cells	Mouse NSC line C17.2	Microfluidic pneumatic based bioprinting	Greater than 90% cell viability was observed with cells migrating towards the fibrin.	[58]
Gellan gum modified with RGD peptide	Primary neural stem cells encapsulated in the scaffold	E18 embryos of BALB/cAr cAusb mice	Handheld microfluidic device	Cells remained viable at 5 days, forming neuronal networks with glial cells	[46]

Table A 2: Plate 1 for flow cytometry.

1 - βT antibody	1 - βT antibody	1 - βT antibody	1 - βT isotype	1 - βT isotype	1 - βT isotype	2 - βT antibody	2 - βT antibody	2 - βT antibody	2 - βT isotype	2 - βT isotype	2 - βT isotype
3 - βT antibody	3 - βT antibody	3 - βT antibody	3 - βT isotype	3 - βT isotype	3 - βT isotype	4 - βT antibody	4 - βT antibody	4 - βT antibody	4 - βT isotype	4 - βT isotype	4 - βT isotype
5 - βT antibody	5 - βT antibody	5 - βT antibody	5 - βT isotype	5 - βT isotype	5 - βT isotype	6 - βT antibody	6 - βT antibody	6 - βT antibody	6 - βT isotype	6 - βT isotype	6 - βT isotype
1 - Nestin antibody	1 - Nestin antibody	1 - Nestin antibody	1 - Nestin isotype	1 - Nestin isotype	1 - Nestin isotype	2 - Nestin antibody	2 - Nestin antibody	2 - Nestin antibody	2 - Nestin isotype	2 - Nestin isotype	2 - Nestin isotype
3 - Nestin antibody	3 - Nestin antibody	3 - Nestin antibody	3 - Nestin isotype	3 - Nestin isotype	3 - Nestin isotype	4 - Nestin antibody	4 - Nestin antibody	4 - Nestin antibody	4 - Nestin isotype	4 - Nestin isotype	4 - Nestin isotype
5 - Nestin antibody	5 - Nestin antibody	5 - Nestin antibody	5 - Nestin isotype	5 - Nestin isotype	5 - Nestin isotype	6 - Nestin antibody	6 - Nestin antibody	6 - Nestin antibody	6 - Nestin isotype	6 - Nestin isotype	6 - Nestin isotype
1 - Olig2 antibody	1 - Olig2 antibody	1 - Olig2 antibody	2 - Olig2 antibody	2 - Olig2 antibody	2 - Olig2 antibody	3 - Olig2 antibody	3 - Olig2 antibody	3 - Olig2 antibody	4 - Olig2 antibody	4 - Olig2 antibody	4 - Olig2 antibody
5 - Olig2 antibody	5 - Olig2 antibody	5 - Olig2 antibody	6 - Olig2 antibody	6 - Olig2 antibody	6 - Olig2 antibody	1 - no stain	2 - no stain	3 - no stain	4 - no stain	5 - no stain	6 - no stain

Table A 3: Plate 2 for flow cytometry.

7 - βT antibody	7 - βT antibody	7 - βT antibody	7 - βT isotype	7 - βT isotype	7 - βT isotype	8 - βT antibody	8 - βT antibody	8 - βT antibody	8 - βT isotype	8 - βT isotype	8 - βT isotype
9 - βT antibody	9 - βT antibody	9 - βT antibody	9 - βT isotype	9 - βT isotype	9 - βT isotype	10 - βT antibody	10 - βT antibody	10 - βT antibody	10 - βT isotype	10 - βT isotype	10 - βT isotype
11 - βT antibody	11 - βT antibody	11 - βT antibody	11 - βT isotype	11 - βT isotype	11 - βT isotype	12 - βT antibody	12 - βT antibody	12 - βT antibody	12 - βT isotype	12 - βT isotype	12 - βT isotype

7 - Nestin antibody	7 - Nestin antibody	7 - Nestin antibody	7 - Nestin isotype	7 - Nestin isotype	7 - Nestin isotype	8 - Nestin antibody	8 - Nestin antibody	8 - Nestin antibody	8 - Nestin isotype	8 - Nestin isotype	8 - Nestin isotype
9 - Nestin antibody	9 - Nestin antibody	9 - Nestin antibody	9 - Nestin isotype	9 - Nestin isotype	9 - Nestin isotype	10 - Nestin antibody	10 - Nestin antibody	10 - Nestin antibody	10 - Nestin isotype	10 - Nestin isotype	10 - Nestin isotype
11 - Nestin antibody	11 - Nestin antibody	11 - Nestin antibody	11 - Nestin isotype	11 - Nestin isotype	11 - Nestin isotype	12 - Nestin antibody	12 - Nestin antibody	12 - Nestin antibody	12 - Nestin isotype	12 - Nestin isotype	12 - Nestin isotype
7 - Olig2 antibody	7 - Olig2 antibody	7 - Olig2 antibody	8 - Olig2 antibody	8 - Olig2 antibody	8 - Olig2 antibody	9 - Olig2 antibody	9 - Olig2 antibody	9 - Olig2 antibody	10 - Olig2 antibody	10 - Olig2 antibody	10 - Olig2 antibody
11 - Olig2 antibody	11 - Olig2 antibody	11 - Olig2 antibody	12 - Olig2 antibody	12 - Olig2 antibody	12 - Olig2 antibody	7 - no stain	8 - no stain	9 - no stain	10 - no stain	11 - no stain	12 - no stain

Table A 4: Flow cytometry on bioink samples 7 days after printing to quantify the cells positive for TUJ1, Nestin and Olig2

Formulation	Marker	%Positive	Standard Deviation
1	TUJ1	3.77	5.34
1	Nestin	68.36	5.30
2	TUJ1	1.36	1.28
2	Nestin	74.24	8.47
2	Olig-2	82.49	0.38
3	TUJ1	0.23	0.17
3	Nestin	81.48	6.08
3	Olig-2	96.67	1.90
4	TUJ1	0.08	0.11
4	Nestin	90.71	6.01
4	Olig-2	80.67	19.13
5	TUJ1	21.73	14.44
5	Nestin	56.88	22.17
5	Olig-2	17.95	12.70
6	TUJ1	14.43	20.41
6	Nestin	96.64	2.91
7	TUJ1	97.47	1.51
7	Nestin	99.12	0.31
7	Olig-2	88.86	12.29
8	TUJ1	98.56	0.48
8	Nestin	97.79	1.39
8	Olig-2	97.79	1.05
9	TUJ1	87.85	7.77
9	Nestin	97.32	2.56
9	Olig-2	95.56	4.45
10	TUJ1	71.71	10.46
10	Nestin	97.64	2.00

11	TUJ1	95.25	2.58
11	Nestin	97.12	1.26
11	Olig-2	99.37	0.89
12	TUJ1	98.74	0.31
12	Nestin	95.29	3.38
12	Olig-2	95.42	5.00

Table A 5: Comparison of cells positive for Tuj1, Nestin, and Olig-2 in each bioink formulation.

Formulation	Tuj1 % positive	Standard Deviation	Nestin % positive	Standard Deviation	Olig-2 % positive	Standard Deviation
Hydrogel A	37.40	38.93	81.76	17.63	73.84	37.95
Hydrogel B	61.13	44.13	93.67	37.16	91.88	7.16
Additive G	29.70	40.08	83.15	15.58	77.40	29.96
Additive P	88.39	10.40	96.84	1.06	96.78	2.24
Additive L	27.50	37.28	90.47	16.51	79.88	34.85
No Additive L	71.03	37.52	84.96	12.24	88.85	8.44